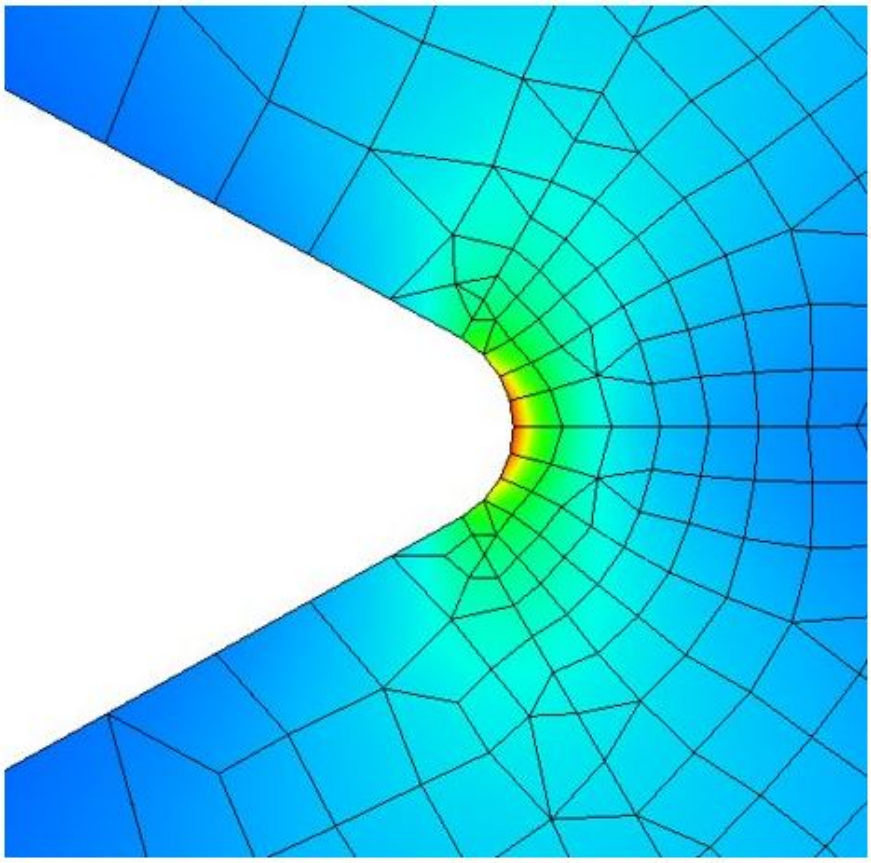

A Method for Predicting Fatigue in Notches Utilizing CAE and the Theory of Critical Distances

Master's thesis in Materials Engineering

WILLIAM HÖGLIND & SIMON LUNDIN

DEPARTMENT OF MECHANICS AND MARITIME SCIENCES

CHALMERS UNIVERSITY OF TECHNOLOGY
Gothenburg, Sweden 2022
www.chalmers.se

Master's thesis 2022

A Method for Predicting Fatigue in Notches Utilizing CAE and the Theory of Critical Distances

WILLIAM HÖGLIND & SIMON LUNDIN

CHALMERS
UNIVERSITY OF TECHNOLOGY

Department of Mechanics and Maritime Sciences
Chalmers University of Technology
Gothenburg, Sweden 2022

A Method for Predicting Fatigue in Notches Utilizing CAE and the Theory of Critical Distances

WILLIAM HÖGLIND & SIMON LUNDIN

Supervisor: Anders Ekberg, Department Mechanics and Maritime Sciences
Supervisor: Per Sjövall, Volvo Cars Corporation
Examiner: Anders Ekberg, Department of Mechanics and Maritime Sciences

Master's Thesis 2022
Department of Mechanics and Maritime Sciences
Report number: 2022:43

Chalmers University of Technology
SE-412 96 Gothenburg
Telephone +46 31 772 1000

Cover: Stress field at a V-notch.

Typeset in LaTeX
Printed by Chalmers Reproservice
Gothenburg, Sweden 2022

A Method for Predicting Fatigue in Notches Utilizing CAE and the Theory of Critical Distances

WILLIAM HÖGLIND & SIMON LUNDIN
Department of Mechanics and Maritime Sciences
Chalmers University of Technology

Abstract

When performing fatigue evaluations, the most critical areas governing the fatigue life of a component are geometrical discontinuities such as notches or sharp corners. Thus, accurate modelling of the geometric discontinuities and their effects is of highest importance to avoid catastrophic failures or overdimensioned components. Today, fatigue evaluations are done mainly utilizing CAE tools, such as FEA, to allow for more precise and complex calculations.

Generally in fatigue design, the guideline is to avoid sharp corners and notches and thereby create robust designs. The first choice of FEA based fatigue evaluation typically overestimates the severity of notches, leading to conservative fatigue predictions. This has the consequence of some design ideas not meeting the fatigue requirements when they in reality might do. The authors therefore investigated methodologies for incorporating FEA with different approaches to fatigue in notches with the aim of producing a less conservative method.

In this report, a methodology for predicting fatigue in sharp corners and notches has been developed. The proposed methodology stems from the Theory of Critical Distances and was verified against available fatigue test data, gathered from four different articles, with good correlation. The methodology was also expanded to allow for fatigue predictions of more complex geometries using virtual test specimen.

Based on the results gained from the method validation it is clear that utilizing the proposed methodology and concepts would decrease the overestimation of notch severity. This allows for an enhanced ability to more accurately assess design ideas.

Keywords: Fatigue, Finite Element, Theory of Critical Distance, Notch

Acknowledgements

First of all, we would like to express our deep graditude to Volvo Cars for granting us this opportunity to work on such an interesting and important subject.
We also extend our deep gratitude towards our supervisors Per Sjövall from Volvo Cars and Anders Ekberg from Chalmers. The time at Volvo Cars under Per Sjövall's guidance has been incredibly educative and we feel grateful for the time, effort and essential input he has given us. Anders Ekberg's lectures on the subject of Fatigue as well as his input and feedback along the way has also been vital for this thesis.

William Höglind & Simon Lundin, Gothenburg, 2022-06-09

Nomenclature

Below is the nomenclature of parameters and variables that have been used throughout this thesis.

b, c	Hardening parameters
D	Sum of damage
E	Young's Modulus
$e_{i,j}$	Strain tensor, linear-elastic solution
$H^{'}, n^{'}$	Ramberg-Osgood material parameters
H_k	k'th slope of multilinear kinematic hardening model
k_{f}	Fatigue notch factor (at the endurance limit)
$k_{\mathrm{f}}^{'}$	Fatigue notch factor (at 1000 cycles to failure)
$k_{\mathrm{f,ref}}$	Fatigue notch factor (at a reference fatigue life)
k_{t}	Stress concentration factor
ΔK_{th}	Crack propagation threshold range
L	Critical distance
m	Reduction factor (at the endurance limit)
$m^{'}$	Reduction factor (at 1000 cycles to failure)
N	Number of cycles
N_{f}	Number of cycles to failure
$N_{\mathrm{f,ref}}$	Reference fatigue life
q	Notch sensitivity
Q_{∞}	Maximum increase of yield surface
r	Distance used in Line, Area and Volume method
R	Stress-ratio
S	Nominal stress

S_{ar}	Nominal stress amplitude of fully reversed cycles
$S_{i,j}$	Stress tensor, linear-elastic solution
S_{n}	Nominal stress (notched specimen)
S_{s}	Nominal stress (smooth specimen)
W_{LE}	Strain energy density, linear-elastic solution
W_{PL}	Strain energy density, elasto-plastic solution
$\boldsymbol{\alpha}$	Backstress
$\dot{\boldsymbol{\alpha}}$	Evolution of backstress
ϵ_{a}	Strain amplitude
$\epsilon_{\mathrm{a,el}}$	Elastic part of strain
$\epsilon_{\mathrm{a,pl}}$	Plastic part of strain
ϵ_{e}	Linear-elastic strain amplitude
$\epsilon_{i,j}$	Strain tensor
$\bar{\epsilon}^{\mathrm{pl}}$	Equivalent plastic strain
$\dot{\bar{\epsilon}}^{\mathrm{pl}}$	Equivalent plastic strain rate
ν	Poisson's ratio
ρ	Notch radius
$\Delta\sigma_{\mathrm{g}}$	Fatigue strength range
σ	Stress
$\boldsymbol{\sigma}, \sigma_{i,j}$	Stress tensor
σ_{a}	Stress amplitude
σ_{ar}	Stress amplitude of fully reversed cycles
σ_{e}	Linear elastic stress amplitude
σ_{eff}	Effective fatigue stress
$\sigma_{\mathrm{f}}^{'}, b, \epsilon_{\mathrm{f}}^{'}, c$	Fatigue parameters
σ_{max}	Maximum tensile stress
σ_{ref}	Reference stress amplitude of notched specimen
$\sigma_{\mathrm{u}}, \sigma_{\mathrm{u}}^{'}$	Ultimate tensile strength
σ_0	Reference stress amplitude of smooth specimen
σ^0	Size of yield surface
$\sigma\vert_0$	Initial size of yield surface
θ	Angle used in Area and Volume method
φ	Angle used in Volume method

Contents

List of Figures

1
Introduction

When structural components are designed, the areas of most interest regarding their fatigue lives are geometric discontinuities such as notches or sharp corners. Thus, accurate modelling of the geometric discontinuities and their effects is of highest importance to avoid catastrophic failures or overdimensioned components. Ever since Wöhler pioneered the field of fatigue analysis in the 1850's, researchers have made improvements to the various models and methodologies regarding notches in fatigue, increasing their complexity, accuracy and efficiency. Today, when designing components with complex geometries, Finite Element Analysis is vastly utilized. Models for material behaviour as well as fatigue analysis are incorporated or coupled with the FEA to allow for more precise and complex calculations. However, increased complexity of the methodologies and models paired with large amounts of loading cycles means an increase in computational power and time as well as cost. This is essentially the ever–present trade off in fatigue predictions.

Generally in fatigue design, the guideline is to avoid sharp corners and notches and thereby create a robust design. Hence, there should be a sufficient safety margin to fatigue failure so that the design is insensitive to manufacturing tolerances. Therefore, the first choice of FEA based evaluation is to not use any special methods for notches. However, often notches and sharp corners cannot be avoided and then this methodology overestimates the severity of stresses and strains in notches, leading to conservative fatigue predictions. The main consequence of the conservative predictions is that it leads to an inability to accurately assess design ideas or concepts where some ideas risk being rejected due to not meeting certain fatigue requirements which they in reality might do. It is clear that in such a competitive industry as the car industry, being able to accurately predict fatigue would give the design teams an edge and opportunities to optimize more attributes of their components. Moreover, considering that the entire car industry is in a transition towards electric propulsion, much of the design work has to be revamped due to the lack of prior solutions, further emphasizing the importance of accurate fatigue evaluations.

In recent years, much work has been done using various approaches with the goal of predicting fatigue in notches accurately. This introduction will cover some advances in the local stress–strain approach as well as approaches utilizing the Theory of Critical Distance (TCD).

In the field of local stress–strain approaches, Ayhan Ince and Grzegorz Glinka developed a computational modeling method, capable of estimating the stress–strain

responses in notch roots [4]. The methodology combines a linear–elastic FEA with a multiaxial Neuber correction coupled with Garud plasticity model. Ince and Glinka later correlated the notch root stress–strain response to fatigue life by developing two variants of a strain–based generalized damage parameter, achieving acceptable to good correlation with fatigue test data obtained from steel, aluminium and nickel–chrome super alloy specimens [5].

Taylor [6] extended the concept of critical distance, originally introduced by Neuber [7] and later simplified by Peterson [8]. This was done by combining FEA with the theory of critical distances where the estimation of the critical distance was based on linear elastic fracture mechanics assumptions. Due to the lacking accuracy of the TCD in the low/medium cycle fatigue regime, Susmel and Taylor [9] considered the critical distance as a variable dependant on the fatigue life instead of a constant material parameter. To calibrate the relationship between the critical distance, L, and the fatigue life, N_f, Susmel and Taylor used the S–N curves of a smooth and notched specimen to find L by iteration. Generally, the relationship between L and N_f shows that at shorter lives, the critical distance is larger. Zhu et.al [10] expanded on the work by Susmel and Taylor by further investigating the effect notch size have on critical distance and fatigue life predictions. The article proposes a methodology coupling a Weibull model with the theory of critical distance which yields good accuracy and shows that a larger notch radius results in a larger critical distance and vice versa.

In this report, the authors will investigate available methodologies for fatigue evaluation and move forward with a methodology which is deemed suitable. This will be done by a first small scale implementation as well as verification of the accuracy by comparison with experimental results. The last goal of the report is to take the first steps to a full–scale implementation of the methodology into the CAE toolbox at Volvo Cars.

2
Theory

In this chapter, background theory for the fatigue evaluation process is presented in three major subsections, notches and stress concentrations, plasticity, and fatigue calculations.

2.1 Notches and Stress Concentrations

Geometrical features such as notches or sharp corners will in any structural component constitute a critical area, more prone to crack initiation, propagation and eventually failure. This is due to the stress being more concentrated in these areas, i.e. they are stress concentrations. In test specimen or other components with well defined geometries, the stress concentration can be described with a factor, k_t. The stress concentration is then defined as the ratio between the local stress σ and the nominal stress:

$$k_\mathrm{t} = \frac{\sigma}{S} \tag{2.1}$$

The stress concentration factor, k_t, can be used to describe the severity of a specific notch. Values for k_t can be found by simply performing a linear elastic FEA and applying equation 2.1. The factor k_t may also be found by using pre–evaluated relations between k_t, the notch radius and the component geometry. An example of this can be seen in figure 2.1, showcasing a relationship between geometry and stress concentration for a notched shaft.

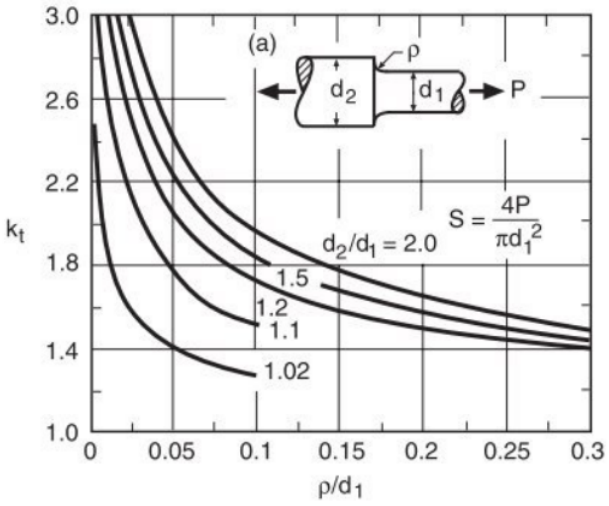

Figure 2.1: Empirical relationship between geometry of notched shaft and k_t. Taken from [1]

In general, k_t increases with a decreasing notch radius. In theory, the stress concentration factor reaches singularity as the radius approaches zero. This phenomenon can be clearly observed in FEA where extremely sharp notches and fine mesh produces stress results resembling the theoretical approach towards infinity.

2.2 Stress Distributions and their Implications

In figure 2.2, a typical stress distribution is shown with the maximum stress located at the surface of the notch root. The stress decreases as the distance from the notch root into the material increases. Also visible in figure 2.2, is the stress gradient at the surface, which is defined as the rate which the stress decreases through the component. With a decreasing notch radius, the gradient increases, meaning the stress decreases quicker with the distance from the notch.

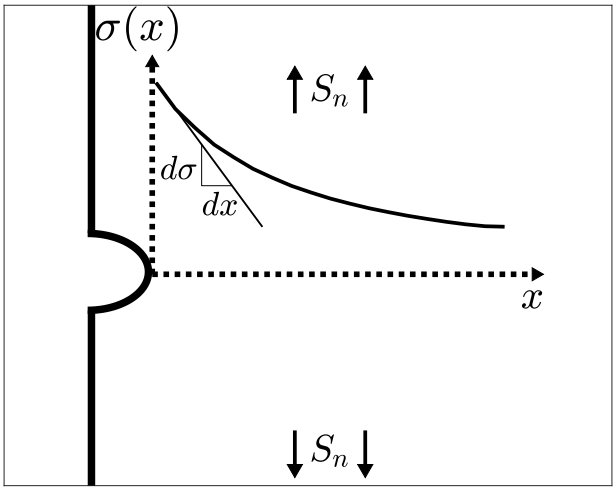

Figure 2.2: Stress distribution with its gradient at a notch with x indicating the distance into the material from the notch root.

It is well known today that the mechanisms behind fatigue damage occur over a small but finite region [1, 11]. This suggests that when addressing fatigue damage using FEA, the stresses and strains in a small but finite region next to the notch surface should be considered instead of the peak stress at the notch root. This is especially important for sharp notches which will inhibit a steeper gradient at the surface of the notch and the stress will drastically decrease with the distance into the material. It follows that the peak stress is less suitable as a fatigue metric for sharp notches.

2.3 Fatigue Notch Factor

When analyzing fatigue test data of notched specimen, it becomes very clear that the theoretical stress concentration factor k_t is a far too conservative metric to base fatigue predictions upon [12, 1]. Assume there are two test specimen, one smooth and one notched. The smooth specimen is loaded so that $\sigma_\mathrm{s} = S_\mathrm{s}$ and the notched as $\sigma_\mathrm{n} = k_\mathrm{t} S_\mathrm{n}$ where the indexes s and n indicates smooth or notched. What the fatigue test data mentioned in the beginning of this paragraph shows is that if the notch stress is the same as the stress in the smooth specimen, $\sigma_\mathrm{n} = \sigma_\mathrm{s}$ the fatigue life differs between the specimen with a difference that increases with reduced notch radius [1]. This phenomenon can be viewed in figure 2.3 where the test data shows that the severity of the theoretical stress concentration, k_t, does not have a corresponding effect on the fatigue life for sharp notches. The underlying causes for this phenomenon are further laid out in section 2.4.1 since they are shared between both the fatigue notch factor and the TCD.

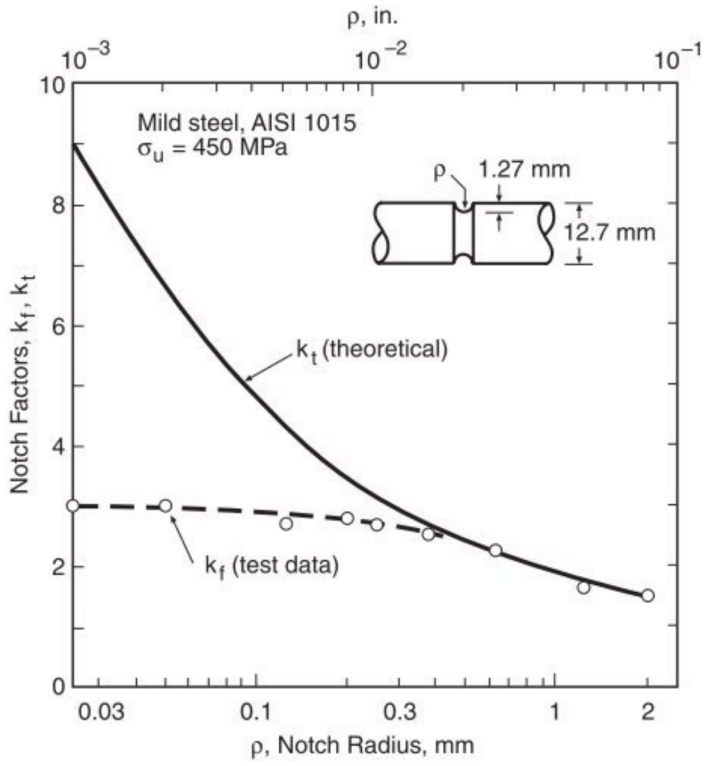

Figure 2.3: Theoretical k_t versus experimentally determined k_f with varying notch radii.Taken from [1], with data from [2].

2.3.1 Definition

The fatigue notch factor, k_f, is meant to represent the 'effective' stress concentration of a notch suitable for evaluating fatigue. It can be defined as the factor that the nominal stress of a notched specimen has to be reduced by in order to have an identical fatigue life to that of a smooth specimen. This relation is shown in equation 2.2 where σ_{ar} is the stress of the smooth specimen and S_{ar} is the nominal stress of the notched specimen. Both stresses correspond the identical fatigue life and the index ar indicates completely reversed cycles.

$$k_f = \frac{\sigma_{ar}}{S_{ar}} \tag{2.2}$$

The effect of the fatigue notch factor varies when comparing different stress levels corresponding to different fatigue lives. This can be viewed in figure 2.4, which shows the S–N curve of a smooth and notched specimen, where the curve for the notch specimen can be considered reduced by the fatigue notch factor from the 'smooth' curve. Since the curves in the logarithmic plot between both specimens are not parallel it follows that the fatigue notch factor is not constant. As shown in figure 2.4 the fatigue notch factor is usually denoted k_f at the endurance limit and k_f' at a fatigue life of 1000 cycles to failure.

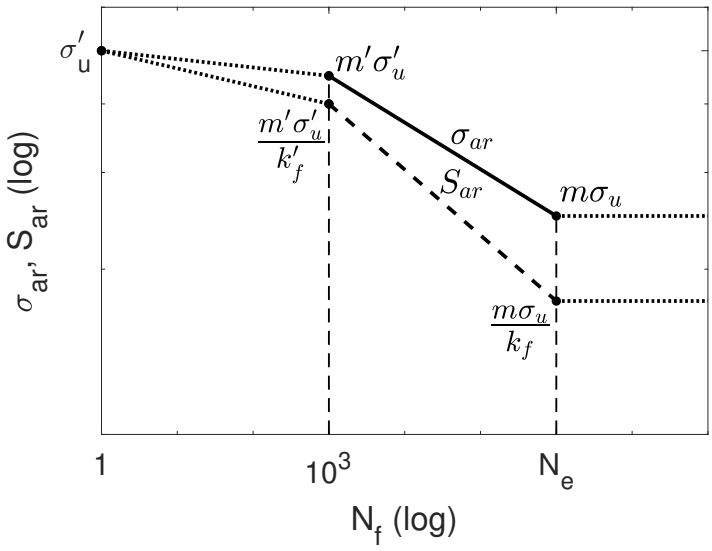

Figure 2.4: S–N curve inspired from [1]. The solid line represents the S–N curve of a smooth specimen and the dashed line represents the S–N curve of a notched specimen.

2.3.2 Calculation

The fatigue notch factor at the endurance limit, k_f, can be determined by modifying the stress concentration factor, k_t, using the notch sensitivity, q, as shown in equation 2.3.

$$k_\mathrm{f} = 1 + q(k_\mathrm{t} - 1) \tag{2.3}$$

q is a parameter ranging between 0 and 1 which is dependant on material type and notch radius. A low notch sensitivity means that the severity of the notch effects are lower and vice versa. The notch sensitivity is defined in equation 2.4 and an estimation of a relation to material and notch radius is shown in figure 2.5. Generally, more ductile materials have a lower notch sensitivity which can be observed in the same figure where the materials are ordered on this basis. From equation 2.4 it follows that a low notch sensitivity produces a larger discrepancy between k_f and k_t.

$$q = \frac{k_\mathrm{f} - 1}{k_\mathrm{t} - 1} \tag{2.4}$$

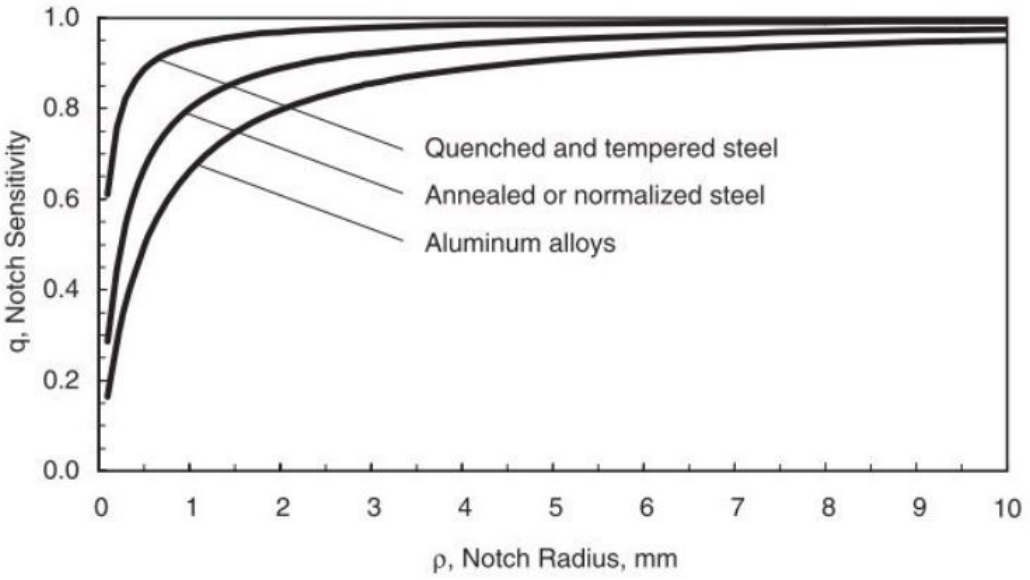

Figure 2.5: The relation between notch sensitivity and notch radius for aluminium and steels. Taken from [1]

The fatigue notch factor at a fatigue life of 1000 cycles, $k_{\mathrm{f}}^{'}$, can be estimated from equation 2.5 where y is extracted from the y–axis of figure 2.6. Once both k_{f} and $k_{\mathrm{f}}^{'}$ have been established it is possible to obtain the fatigue notch factor at any given fatigue life in between 1000 cycles to failure and the endurance limit. This is done using linear interpolation. The fatigue notch factor at an arbitrary fatigue life is designated $k_{\mathrm{f,ref}}$ in this thesis, 'ref' representing referenced fatigue life.

$$k_{\mathrm{f}}^{'} = 1 + y(k_{\mathrm{f}} - 1) \tag{2.5}$$

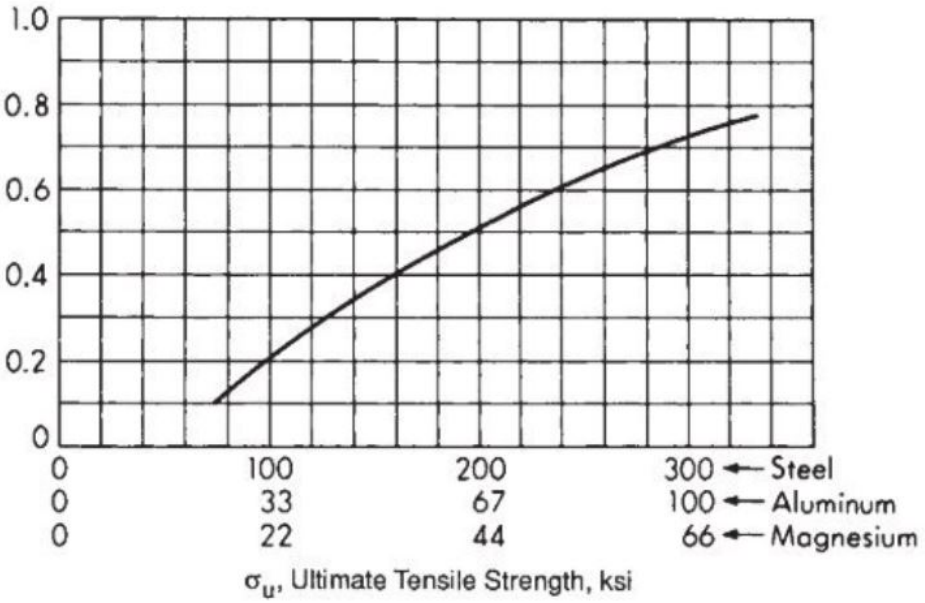

Figure 2.6: Curve based on empirical data that uses material parameters in order to estimate the fatigue notch factor at 1000 cycles to failure. Taken from [1]

2.4 Theory of Critical Distances

Another concept for considering the stress gradient is the Theory of Critical Distances (TCD). There are multiple methods originating from the TCD, which is based upon the introduction of the critical distance L as a material specific parameter. The methods are, from simpler to more complex, the Point Method (PM), Line Method (LM), Area Method (AM) and Volume method (VM). TCD was originally introduced by Taylor when he connected the previously mentioned four methods through the material parameter L [6, 13]. However, Neuber [7] did take the first step in 1958, when he averaged the elastic stress along a specific distance from the notch root, and thus invented the LM. Today that distance of which the stress is averaged over in the LM is $2L$ [13, 14]. One year later, R.E Peterson invented the PM when he achieved accurate estimations of fatigue life by considering the stress at a distance, now known as $L/2$, from the notch root as the effective stress used in the fatigue calculations [8, 14]. Taylor introduced the AM by using the average stress over an area from the notch root [15], while the VM was established by Daniel Bellett, Taylor et al. where the stress instead was averaged over a volume in front of the notch root [16].

The failure criterion for each method under the TCD umbrella is stated as the following for PM, LM, AM and VM respectively [13]:

$$\text{PM: } \sigma_{eff} = \sigma(L/2) \tag{2.6}$$

$$\text{LM: } \sigma_{eff} = \frac{1}{2L}\int_0^{2L} \sigma(r)dr \tag{2.7}$$

$$\text{AM: } \sigma_{eff} = \frac{2}{\pi(1.32L)^2}\int_{-\frac{\pi}{2}}^{\frac{\pi}{2}}\int_0^{1.32L} \sigma(r,\theta)rdrd\theta \tag{2.8}$$

$$\text{VM: } \sigma_{eff} = \frac{3}{2\pi(1.54L)^3}\int_0^{\pi}\int_{-\frac{\pi}{2}}^{\frac{\pi}{2}}\int_0^{1.54L} \sigma(r,\theta,\varphi)r^2 sin(\theta)drd\theta d\varphi. \tag{2.9}$$

The parameter L can be experimentally determined or estimated as:

$$L = \frac{1}{\pi}\left(\frac{\Delta K_{\text{th}}}{\Delta\sigma_{\text{g}}}\right)^2, \tag{2.10}$$

where ΔK_{th} is the crack propagation threshold range and $\Delta\sigma_{\text{g}}$ is the fatigue strength range. However, as have become clear in the recent years, the critical distance, L, should not be interpreted as only a constant material parameter. Rather, the critical distance seems to also be dependant on both the notch geometry and the fatigue life, N_{f} [9, 10, 14]. Susmel and Taylor proposes a methodology for estimating L using the Wöhler curve of a smooth and a notched specimen. The procedure begins with an initial fatigue life guess, N_{ref}. Both Wöhler curves has a corresponding nominal stress magnitude for this fatigue life: σ_0 for the smooth one, and σ_{ref} for the notched one as shown in figure 2.7. The next step is to perform a linear elastic FEA of the notched specimen with a nominal stress of σ_{ref}. Focusing on the stress distribution at the notch using the FEA results where x is the distance from the notch root into

the material, we find $L/2$ at the point where $\sigma(x) = \sigma_0$. Figure 2.8 visualizes this procedure. By using the stress–strain state at a distance of $L/2$ from the notch root, the fatigue life, N_f, is estimated. If $N_\mathrm{f} = N_\mathrm{f,ref}$ is within a small error margin, no further iterations are needed and the calibrated critical distance is found. However, if $N_\mathrm{f} \neq N_\mathrm{f,ref}$, the procedure is iterated again with updated $N_\mathrm{f,ref}$ until convergence is found [9].

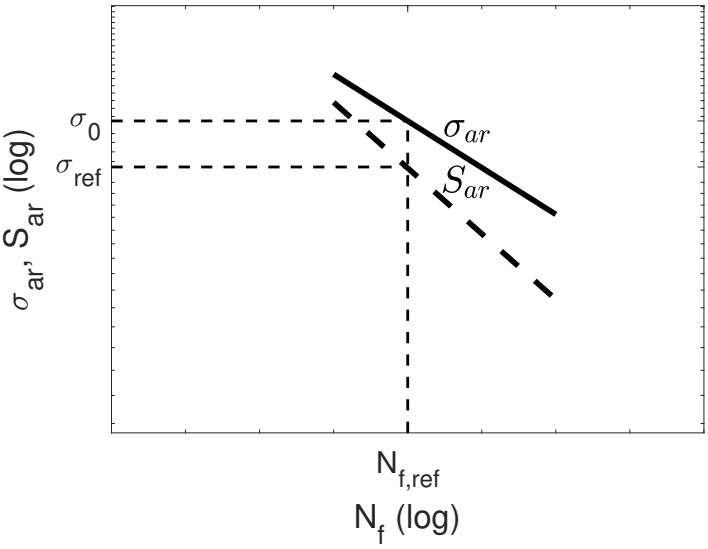

Figure 2.7: S–N curves for smooth and notched specimen, based on figure 2.4, with reference life and corresponding nominal stresses.

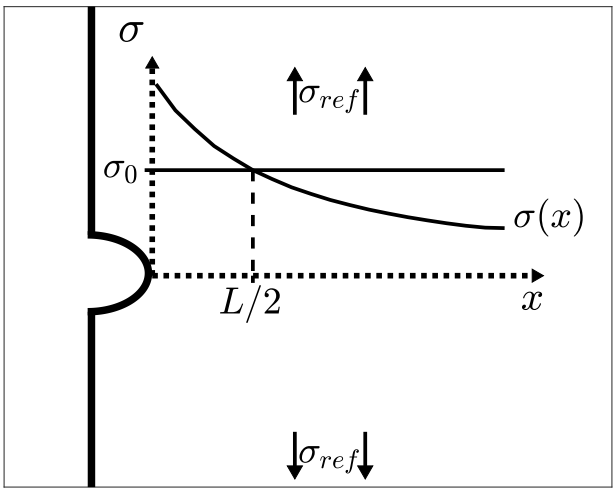

Figure 2.8: Stress distribution at notch, with $L/2$ found at the intersection between σ_0 and $\sigma(x)$.

2.4.1 Underlying Causes

Both the fatigue notch factor and TCD approaches aim at finding the effective stresses and strains suitable for fatigue evaluation. These effective values are not necessarily the highest stresses and strains found in the notch, especially for sharp corners as shown in figure 2.3. The section will highlight some of the underlying causes for why this is the case.

Fatigue cracks are initiated at, and often propagate along, weaker regions of the material. These weaker regions involve but are not limited to surface scratches, inclusions, voids or microstructural stress concentrations. The highly stressed volume at the notch may not inhibit any weaker regions and thus the crack grows slower than what would be expected [1]. This can be compared to a smooth specimen where the highest stresses are found over a much larger volume where the crack has a higher risk of initiating at a weaker region. This phenomenon is thoroughly documented in literature [17, 18, 19]. Dowling showcases this effect with the help of a figure in his book [1], which can be seen in figure 2.3.

In section 2.2 the stress distribution and its implication is explained. The steep gradient associated with sharp notches together with the concept of fatigue mechanisms occurring over a small region suggests that consideration should be made for the stress distribution away from the notch. And not accounting for the stress distribution in sharp notches will according to Topper et.al. result in overestimating the stress concentrations impact on fatigue life which will lead to unnecessarily conservative results [12].

2.5 Plasticity

As mentioned in the introduction, there is always a trade–off between complexity and calculation time in FEA. One aspect which greatly impacts the calculation time is the chosen material model. A complex model with precise modelling of the material's cyclic plastic response is an example of a factor greatly prolonging the calculation. In this section, various methods for considering local plasticity at the notch are accounted for.

2.5.1 Neuber Rule

The Neuber Rule simply states that below plastic yielding the elastic stress concentration factor k_t is equal to the geometric mean of the actual stress and strain concentration factors [20]. This produces the relationship between the elastic stress and strain, σ_e and ϵ_e, and actual stress and strain, σ_a and ϵ_a, as presented in equation 2.11. The authors define 'actual stress and strain' to constitute that consideration for plasticity has been made. It is also possible to express the product of elastic stress and strain using the nominal stress, S, as expressed on the right in equation 2.11.

$$\sigma_{\mathrm{a}}\epsilon_{\mathrm{a}} = \sigma_{\mathrm{e}}\epsilon_{\mathrm{e}} = \frac{(k_{\mathrm{t}}S)^2}{E} \tag{2.11}$$

The cyclic stress–strain curve is commonly represented by the Ramberg–Osgood form [1] and is shown in equation 2.12. Together with equation 2.11 it is possible to translate the linear elastic stress and strain to 'actual' stresses and strains [1]. This is illustrated graphically in figure 2.9 where the linear elastic stress–strain relationship is translated onto the Ramberg–Osgood form, eq. 2.12, using the parabolic function, equation 2.11. The resulting stress and strain, σ_{a} and ϵ_{a}, has an elasto–plastic stress–strain relationship.

$$\epsilon_{\mathrm{a}} = \frac{\sigma_{\mathrm{a}}}{E} + \left(\frac{\sigma_{\mathrm{a}}}{H'}\right)^{1/n'} \tag{2.12}$$

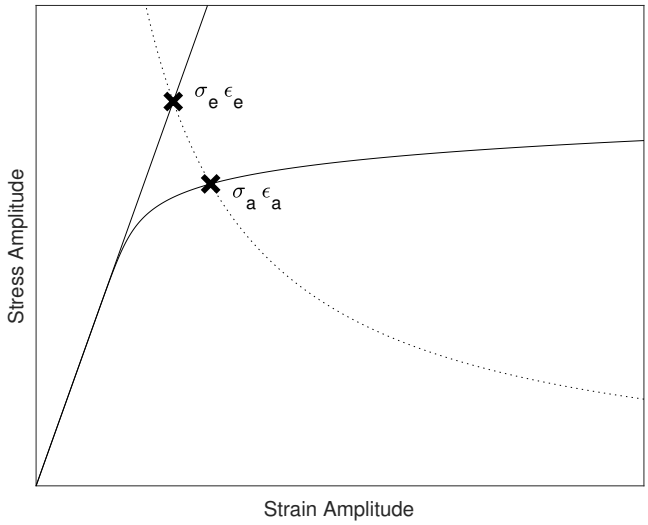

Figure 2.9: Diagram of plotted linear elastic stress–strain relationship together with the Ramber–Osgood form. The parabolic function in equation 2.11 is shown as the dotted line, which is used to translate the linear elastic values onto the Ramberg–Osgood form

Sharpe et al. [21] and Knop et al. [22] compared among others, the Neuber Rule and the energy density approach proposed by Glinka and arrived at the conclusion that the Neuber rule is best under plane stress conditions.

2.5.2 Energy Density Approach

Another approach of evaluating the elasto–plastic stresses and strains near notches is the energy density approach presented by Glinka [23]. Similar to Neuber's rule it uses a linear elastic stress and translates this onto a cyclic elasto–plastic curve in the form of Ramberg–Osgoods relation as shown in eq 2.12. The method proposed by Glinka does this by concluding that the strain energy density due to the local stress

field in the linear elastic solution, W_{LE}, is equal to that of the plastic zone at the notch, represented by the elasto–plastic solution, W_{EP}. This is shown in equation 2.13 where the linear elastic case is on the left, and the elasto–plastic case on the right hand side.

$$\begin{aligned} W_{\mathrm{LE}} &= W_{\mathrm{EP}} \\ \int_0^{e_{ij}} S_{ij} de_{ij} &= \int_0^{\epsilon_{ij}} \sigma_{ij} d\epsilon_{ij} \end{aligned} \tag{2.13}$$

Glinka's [23] proposed method further distinguishes between the conditions of plane stress and plane strain. Comparisons made by Sharpe et al. [21] and Knop et al. [22] between different methods, including Neuber and Glinka, showed that Glinkas proposed method produced more accurate results under plane strain conditions.

2.5.3 Cyclic Plasticity

Estimating a realistic cyclic plasticity response of a material means an accurate modelling of the cyclic hardening or softening as well as capturing the Bauschinger effect [1]. There are mainly two types of hardening models relevant for metals, isotropic and kinematic, where the latter is the one more widely used in the industry due to its capability of predicting the Bauschinger effect [1] and the flawed realism of the isotropic hardening model. However, each material could be considered to inhibit a combination of the two mechanisms where generally the kinematic part is more prevalent. Thus, the preferred hardening models are either a kinematic or a combined kinematic and isotropic hardening model.

There is a plethora of different models describing the two hardening mechanisms. In isotropic hardening, the size of the yield surface increases while its center remains in the origin. This is, in the ABAQUS user guide [3], described with the following model:

$$\sigma^0 = \sigma|_0 + Q_\infty \left(1 - e^{-b\bar{\epsilon}^{\mathrm{pl}}}\right) \tag{2.14}$$

where Q_∞ is a material parameter describing the maximum increase of the yield surface, b is a material parameter describing at which rate the yield surface is increasing, and $\bar{\epsilon}^{pl}$ the equivalent plastic strain.

Kinematic hardening does not increase the size of the yield surface σ^0. Instead, the yield surface is translated along the direction in which the hardening inducing stresses are acting. Similarly, this could be described by a flow rule for linear kinematic hardening known as the Ziegler hardening law which ABAQUS uses [3]:

$$\dot{\boldsymbol{\alpha}} = C \frac{1}{\sigma^0} (\boldsymbol{\sigma} - \boldsymbol{\alpha}) \dot{\bar{\epsilon}}^{\mathrm{pl}} \tag{2.15}$$

where $\dot{\boldsymbol{\alpha}}$ describes the evolution of the backstress $\boldsymbol{\alpha}$, which in turn represents the center of the yield surface. Further, C is the kinematic hardening modulus.

The Ziegler hardening law can be further expanded upon to form a multilinear kinematic hardening model where the plastic portion of the stress–strain curve is described by multiple linear portions with different slopes [3]:

$$H_k = \frac{\sigma_{k+1} - \sigma_k}{\epsilon_{k+1}^{\mathrm{pl}} - \epsilon_k^{\mathrm{pl}}} \tag{2.16}$$

where H_k is the slope of the stress strain curve between data points k and $(k+1)$.

Ideally, cyclic loading experiments would be conducted on each material used in engineering components to find the necessary parameters. Data points along the stabilized cyclic curve or of the tensile test curve could be used as input for the hardening models used by ABAQUS. However, as mentioned earlier this would simply be far too time consuming and expensive, especially considering the existence of already published work on a large amount of materials. Boller and Seeger's book collection [24, 25] is an example of this showing that common material and fatigue parameters such as H', n', σ_{f}', ϵ_{f}', b and c can be found for many engineering materials. While none of these parameters could be used directly as input to ABAQUS's plasticity models, H' and n' which is used to describe the plastic part of equation 2.12 shown below in equation 2.17, could be used to determine the points needed as input for ABAQUS's built in stabilized cyclic curve parameter calibration. The points should be in the form of stress and plastic strain.

$$\epsilon_{\mathrm{a,pl}} = \left(\frac{\sigma_{\mathrm{a}}}{H'}\right)^{1/n'} \tag{2.17}$$

$$\epsilon_{i,\mathrm{pl}} = \epsilon_i - \frac{\sigma_i}{E} - \epsilon_{\mathrm{pl}}^0 \tag{2.18}$$

The points required for the calibration, are defined according to equation 2.18, where ϵ_i^{pl} is the plastic strain, ϵ_i the total strain and σ_i the stress at the i'th point. ϵ_{pl}^0 is set as the resulting strain when the applied stress is 0.

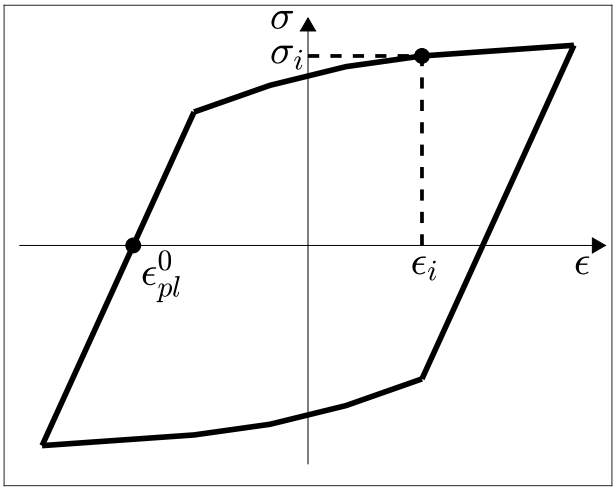

Figure 2.10: Stabilized cycle with points of stress and strain relevant to the parameter calibration. Inspiration from [3]

2.6 Fatigue Predictions

With the local stress and strain response obtained from load histories, material models etc. the expected life of the component can be estimated. Just as there are several different methods to calculate the stress–strain response, there are several methodologies available for engineers to estimate the fatigue life.

2.6.1 High/Low Cycle Fatigue

Depending on the type of component and its application, fatigue failure might in one case be expected to occur after just several cycles while in another case after millions of cycles. In the first case it can be expected to involve a lot of plasticity due to the higher magnitude of loading. Meanwhile, in the second case, where the component lasted for millions of cycles, one can expect there to be very minor plasticity limited to the tip of the fatigue crack [1]. These are the characteristics of low– and high cycle fatigue. The shift from low– to high cycle fatigue (LCF and HCF) typically ranges between 10^2 to 10^4 cycles depending on material. Consideration of plasticity in the fatigue analysis is more vital in LCF whereas it in most cases might be negligible in HCF. While the stress based approach in HCF utilizes stress versus fatigue life curves the strain based approach more suitable for LCF uses strain versus fatigue life curves. However the Wöhler curves may not only be strain or stress based which will be further elaborated upon in section 2.6.2.

Plotting stress–based fatigue test data in a log–log plot, the points often form a straight line where the stress either could be nominal, S_a, or in the form of actual local stress amplitude, σ_a. In the case of actual local stresses, the straight line is

often described by equation 2.19, where $\sigma_{\mathrm{f}}^{'}$ and b are material parameters to be fitted.

$$\sigma_{\mathrm{a}} = \sigma_{\mathrm{f}}^{'}(2N_{\mathrm{f}})^{b} \tag{2.19}$$

Similarly the elastic strain amplitude $\epsilon_{\mathrm{a,el}}$ could simply be described as σ_{a}/E, meaning its relationship to fatigue life is as follows:

$$\epsilon_{\mathrm{a,el}} = \frac{\sigma_{\mathrm{f}}^{'}}{E}(2N_{\mathrm{f}})^{b}, \tag{2.20}$$

whereas the plastic strain amplitude relates to the fatigue life according to equation 2.21.

$$\epsilon_{\mathrm{a,pl}} = \epsilon_{\mathrm{f}}^{'}(2N_{\mathrm{f}})^{c} \tag{2.21}$$

Through a combination of equation 2.20 and 2.21 we form the Coffin–Manson relationship which is more suitable, although not exclusively, to LCF:

$$\epsilon_{\mathrm{a}} = \frac{\sigma_{\mathrm{f}}^{'}}{E}(2N_{\mathrm{f}})^{b} + \epsilon_{\mathrm{f}}^{'}(2N_{\mathrm{f}})^{c} \tag{2.22}$$

2.6.2 Damage Parameters

Translation between a stress–strain response and the corresponding fatigue life and fatigue damage is often done through equalization of damage parameters and fatigue life curves [5]. Examples of different damage parameters have already been shown as the left side of equations 2.19-2.22. The parameters range in complexity from the simple uniaxial stress or strain amplitude as explained in section 2.6.1 to a set of various equivalent stress or strain states. Ayhan Ince has in his PHD thesis listed various stress–, strain– and energy based damage parameters [26].

2.6.3 Loading and Mean Stress Corrections

No matter how accurate and reliable the fatigue analysis methodology is, the results are only as reliable as the least reliable input. Material parameters, for example, might be gathered from a very limited amount of experiments resulting in uncertainties in the parameters and by extent the stress–strain response of the material. The type and magnitude of loading is an other factor which is of high importance to describe accurately. The most advanced fatigue analysis methodology will still provide inaccurate results if the loading conditions were not properly analyzed and implemented in the analysis. For uni–axial loading the authors identified the consideration of mean stresses to be of great importance. This is laid out in the following paragraphs. Mean stresses can be presented through the stress ratio $R = \sigma_{\mathrm{min}}/\sigma_{\mathrm{max}}$ [1, 27], the value of $R = -1$ corresponding to a reversed loading cycle while $R > -1$ indicates an introduced positive mean stress and vice versa. It follows that an introduced mean stress will result in higher maximum (tensile or compressive) stress which might lead to more detrimental effects. In contrast, compressive mean stresses generally increases the fatigue life of the component [28, 29]. Mean stresses can be

introduced in different ways, including formation of residual stresses, by e.g. shot peening or overloading, or by simply having a non–reversed loading case.

One simple way of considering mean stress in the stress based approach is by the Smith, Watson and Topper equation which could be written in either form as shown in equation 2.23. Here, σ_{ar} stands for the stress amplitude of a reversed cycle of equivalent damage to a cycle of amplitude σ_{a} with the largest tensile stress σ_{max}. This equivalent stress amplitude can then be employed in a stress vs fatigue life curve.

$$\begin{aligned} \sigma_{\mathrm{ar}} &= \sqrt{\sigma_{\mathrm{max}}\sigma_{\mathrm{a}}} \\ \sigma_{\mathrm{ar}} &= \sigma_{\mathrm{max}}\sqrt{\frac{1-R}{2}} \end{aligned} \tag{2.23}$$

Accounting for mean stress in a strain based approach to fatigue can be done by altering the Coffin–Manson relation shown in equation 2.22. One approach is the Modified Morrow Approach, presented in equation 2.24, where the elastic part of the expression have been altered by adding a mean stress dependence with σ_{m} representing the mean stress [30]. This will have the effect of accounting for mean stress at HCF while diminishing the same effect for relatively short lives.

$$\epsilon_{\mathrm{a}} = \frac{\sigma_{\mathrm{f}}^{'}}{E}\left(1 - \frac{\sigma_{\mathrm{m}}}{\sigma_{\mathrm{f}}^{'}}\right)(2N_{\mathrm{f}})^{b} + \epsilon_{\mathrm{f}}^{'}(2N_{\mathrm{f}})^{c} \tag{2.24}$$

The method by Smith, Watson and Topper (SWT) [31] suggests another alteration of the Coffin–Manson relation as presented in equation 2.25.

$$\sigma_{\mathrm{max}}\epsilon_{\mathrm{a}} = \frac{\left(\sigma_{\mathrm{f}}^{'}\right)^{2}}{E}(2N_{\mathrm{f}})^{2b} + \sigma_{\mathrm{f}}^{'}\epsilon_{\mathrm{f}}^{'}(2N_{\mathrm{f}})^{b+c} \tag{2.25}$$

Dowling argues that the SWT approach produces acceptable results for both aluminium and steel [1].

2.6.4 Palmgren Miner

One method commonly used in industry when estimating the fatigue life is the Palmgren–Miner rule introduced in the early 1920's. It utilizes a damage parameter vs cycles to failure curve of a material where, for a specific amplitude and mean stress, the cycles to failure, N_{f}, can be determined. The damage can then be calculated as the number of cycles applied with that specific load case, N, over N_{f}.

$$D = \frac{N_1}{N_{1\mathrm{f}}} + \frac{N_2}{N_{2\mathrm{f}}} + \frac{N_3}{N_{3\mathrm{f}}} + \ldots = \sum \frac{N_i}{N_{i\mathrm{f}}} = 1 \tag{2.26}$$

As equation 2.26 states, it is possible to establish the damage from a load sequence by sorting the cycles by damage parameter into blocks where each block contain all identical cycles. The damage for each block can be calculated as mentioned before where the total damage, D, is the sum of the damage of all different blocks. Failure occurs in theory at 100 % damage, corresponding to $D = 1$. However, this rule

does not consider the order in which the blocks of loading cycles are applied to the component. In other words, sequencing effects prolonging or shortening the fatigue life depending on the order of which specific blocks of loading cycles are applied are not considered [32].

3
Results

3.1 Method Development – Simple Geometry

The methodology proposed by the authors in this report is similar to the method proposed by Susmel and Taylor [9]. In order to acquire the critical distance for a component, of a specific material and load case, S–N curves of smooth and notched specimens are employed. Susmel and Taylor acquire these curves through fatigue testing which can be both time consuming and expensive. Therefore, the authors of this report investigated the possibility to instead construct the necessary elements of these curves through material and geometrical parameters accompanied by FEA.

3.1.1 Proposed Critical Distance Calculation

As laid out in section 2.4, the critical distance calculated from this approach solely depends on the fatigue notch factor, between the smooth and notched S–N curves, assuming similar surface roughness. And the fatigue notch factor does not require the S–N curves to be known but can instead be estimated through material and geometrical parameters. So without knowing the S–N curves it is possible to make the assumption that a notched specimen has to have its nominal stress reduced by the fatigue notch factor, $k_{\mathrm{f,ref}}$, in order to have a similar fatigue life to that of a smooth specimen. The critical distance can then be determined by investigating the stress distribution of the smooth specimen with nominal stress, S_{s}, and the notched specimen with a nominal stress of $S_{\mathrm{n}} = S_{\mathrm{s}}/k_{\mathrm{f,ref}}$. Since the analysis of the stress distribution is done using linear elastic FEA the magnitude of the distributions scales linearly with applied nominal stress. It follows that the magnitude of S_{s} does not affect the length of the critical distance since both stress distributions are identically scaled, meaning the 'intersection' between both distributions is only altered vertically in a stress vs 'distance away from the notch' diagram such as figure 2.8. Simply put, the critical distance is solely dependant on $k_{\mathrm{f,ref}}$ where an arbitrary value of S_{s} is used to calculate the critical distance.

In section 2.3.2 the procedure to find $k_{\mathrm{f,ref}}$ at any arbitrary fatigue life is presented. Using $k_{\mathrm{f,ref}}$ to calculate the critical distance is done by a slight modification of figure 2.8. Applying an arbitrary nominal stress, notated σ_{ref} in the figure, the point in the stress distribution where $\sigma(x) = k_{\mathrm{f,ref}}\sigma_{\mathrm{ref}}$, is located at a distance of $L/2$ away from the notch root.

3.1.2 Proposed Methodology for Fatigue Evaluation

In figure 3.1, a flowchart depicting the fatigue evaluation procedure is shown. The first step in the flowchart is visualized as a beige input/output arrow. Here, an FE–model of the investigated component is constructed. For simplification purposes, the mesh at the notch(es) of interest should be constructed so that nodes are evenly distributed along a distance into the component along the normal to the plane inhibiting the maximum principal stress. An example of a mesh at a notch is shown in figure 3.2 where the blue lines are located on both sides of the line with the evenly distributed nodes marked as white crosses. The appropriate load type has to be applied to the model. However, the magnitude of the load could be chosen arbitrarily due to this being a scalable linear elastic evaluation. The material parameters required for a linear elastic FEA are the Young's modulus, E and Poisson's ratio ν. Plotting the stress over the nodes recently described as white crosses in figure 3.2 reveals a stress distribution much alike the one in figure 2.2.

The next step is calculating the fatigue notch factor, $k_{\mathrm{f,ref}}$. One of the inputs needed for this is an initial fatigue life guess, $N_{\mathrm{f,ref}}$. Due to the way the iteration process converges, an initial guess of the endurance limit will suffice. In other words, this initial guess is not very crucial for the iteration process. The other parameters needed to calculate $k_{\mathrm{f,ref}}$ are the notch sensitivity, q, and the ultimate tensile strength, σ_{u}. At first, k_{f} at the endurance limit and $k_{\mathrm{f}}^{'}$ at 1000 cycles are calculated according to section 2.3.2. With the fatigue notch factor found at these two fatigue lives, $k_{\mathrm{f,ref}}$ is easily found by interpolation. Using the interpolated $k_{\mathrm{f,ref}}$, $L/2$ is found according to section 2.4 with the modifications provided in the previous section 3.1.1. Depending on the initial guess, ththe calculated $L/2$ will most likely either be too conservative, i.e. too short or too non–conservative, i.e. too long. FEA results obtained through the application of an arbitrary unit load are now scaled accordingly to the load history which will be investigated. This would result in a pseudo–elastic stress distribution as the one mentioned earlier. From this distribution, at a distance of $L/2$ from the surface along the line of nodes, the stress–strain state should be used to identify pseudo–elastic amplitudes of stress and strain and mean stresses. In cases with variable amplitude loading, rainflow–counting [1, 33] could be utilized. These pseudo–elastic values should in the next step be translated into elasto–plastic values via the Neuber correction from section 2.5.1. For this, the material parameters H' and n' are necessary. Identifying the damage parameters from the Neuber corrected stress state at a distance of $L/2$ from the notch tip provides the possibility to predict a fatigue life, N_{f}, given the fatigue parameters $\sigma_{\mathrm{f}}^{'}$, b, $\epsilon_{\mathrm{f}}^{'}$ and c are known. If $N_{\mathrm{f}} = N_{\mathrm{f,ref}}$, no iterations are needed. If $N_{\mathrm{f}} \neq N_{\mathrm{f,ref}}$ which often is the case, the procedure is iterated again, with $N_{\mathrm{f,ref}} = N_{\mathrm{f}}$ until the critical distance together with the predicted N_{f} has converged.

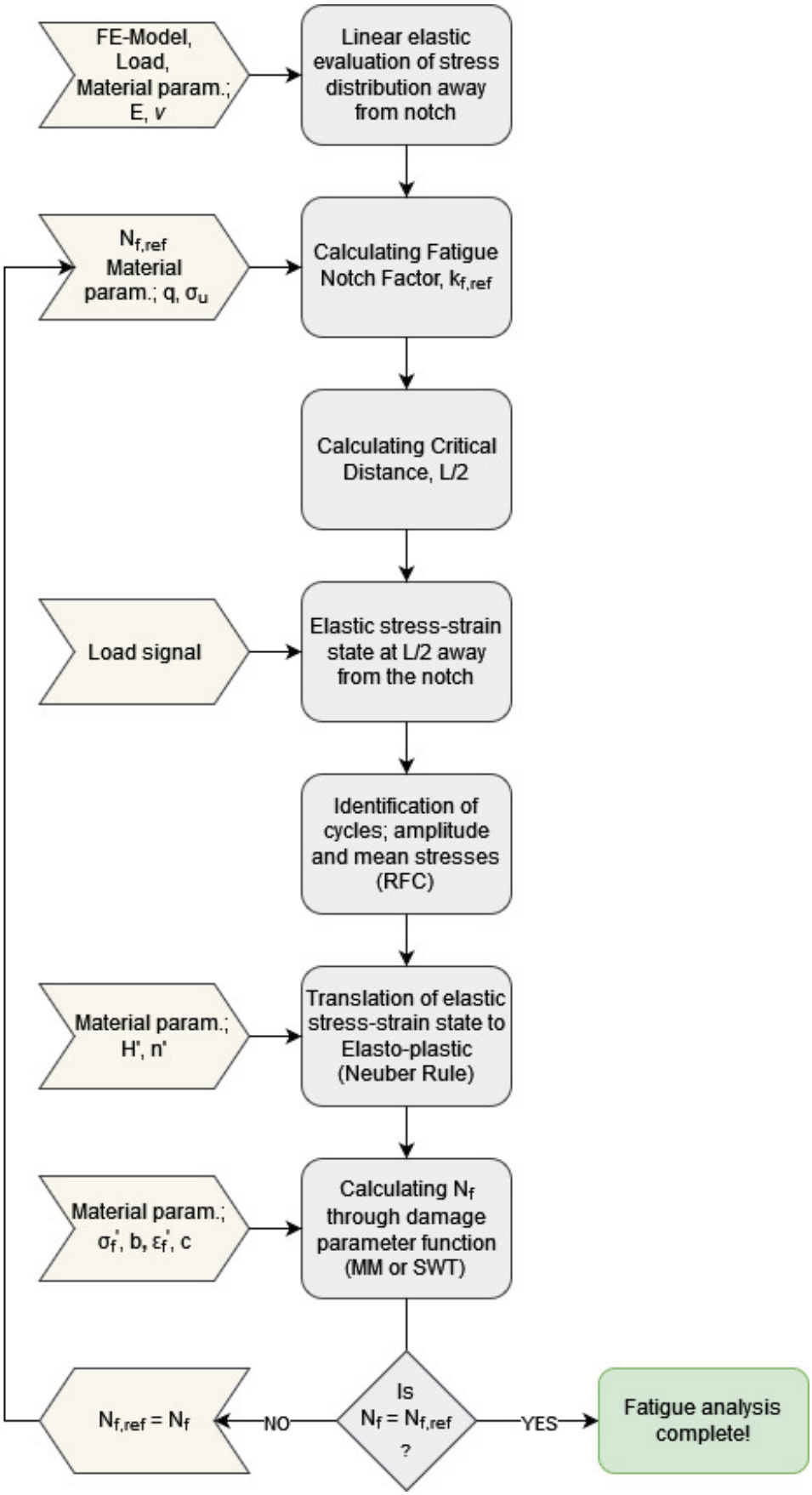

Figure 3.1: Flowchart

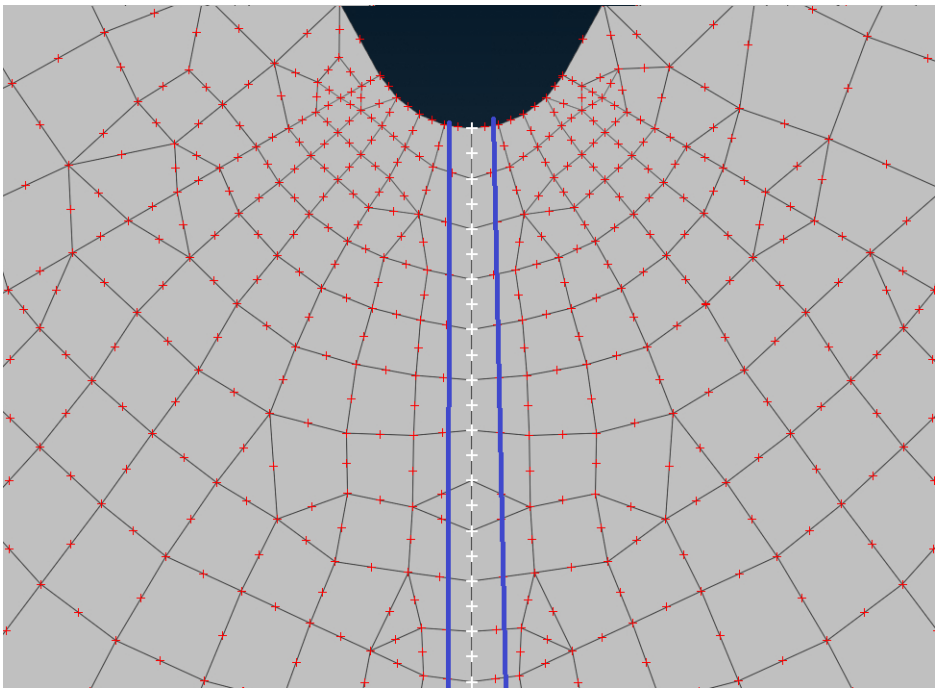

Figure 3.2: Notch mesh

3.1.3 Elasto–Plastic Alternative

In ABAQUS and other similar software, there is a possibility to perform FEA using a plasticity model with the goal of achieving a more accurate material response. The drawback however, as mentioned in the introduction, is the added computational power needed when performing elasto–plastic FEA. Therefore, it is of high interest to know how much of a benefit there is, if any, to adding a plasticity model and at what time–wise cost that is done.

The procedure just described in section 3.1.2 with figure 3.1 needs to be slightly expanded to allow for elasto–plastic FE evaluation. Given the linear–elastic analysis has already been performed, the first step would be to calibrate parameters for a plasticity model in ABAQUS. Instead of a single load, an appropriate loading sequence containing several cycles should be applied to capture the hardening effects of the plasticity model and allow for stabilization. After running the elasto–plastic FEA, stress and strain amplitudes as well as mean stresses should be identified just like in the linear–elastic analysis. The main difference between this approach and the linear–elastic one is that the plastic one utilizes the converged critical distance already calculated for the applied nominal stress amplitude from the linear elastic methodology. This means no further iteration is needed. Finally, the identified damage parameters at $L/2$ from the notch tip could be used to estimate the fatigue life.

3.2 Case Studies

With a proposed methodology laid out, the next step is validation. A MATLAB script has been written, capable of converting pseudo–elastic FEA results into Neuber corrected stress–strain response histories which then will be used in conjunction with the script containing the proposed methodology. The authors have also included an option for using multiple cycles of elasto–plastic FEA results in the written script, to allow for comparison between Neuber corrected results and results gained by utilizing the more complex plasticity models included in ABAQUS.

Validation will be done through comparison of real fatigue test data found in the literature, by first modelling of test specimen with the geometry obtained from the articles, performing FEA on the modelled test specimen using the provided material parameters. In cases where some parameters might be missing, other reliable sources will be used. In order for the authors of this report to assess the accuracy of material parameters, information about the material and specimen used in the article is vital. Heat treatment, processing method and surface finish of the specimen are examples of factors which influence material parameters. Sources containing material parameters should therefore ideally have calibrated their parameters with a strong match of these factors with the article containing the fatigue test data.

Four different articles were chosen from the literature as basis for the method validation [34, 35, 36, 37]. Each article includes specimen geometry, fatigue test data and basic material parameters. These four articles were chosen to provide a variety of different factors such as specimen shape, notch type, notch radius, loading case as well as material which hopefully will give opportunities to draw conclusions related to these factors.

3.2.1 FE–Models

The first step of the validation process is to model the specimen using ANSA as pre–processor. The specimens will in the remainder of this report be referred to model A, B, C and D. Model A is found in an article by Yang et al. [34]. The geometry of this model was cut in half and a symmetry condition was applied to the cut edge. Reducing the size of the model in this manner allows for faster computation without sacrificing precision. The resulting FE–model is presented in figure 3.3. Similar procedure was preformed when FE–modelling the other case study models where the model sizes were reduced by either 50 or 75 %. Model B can be seen in fig 3.4, C in fig 3.5 and D in fig 3.6.

Model A

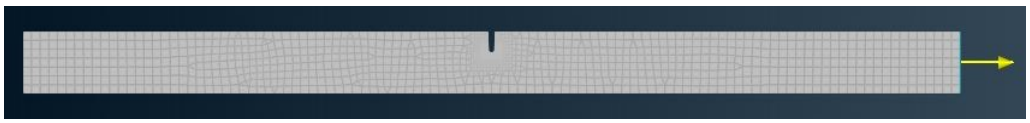

Figure 3.3: Plate made out of 7075–T6 Aluminium with a u–notch of radius 1.45 mm subjected to cyclic axial loading.

Model B

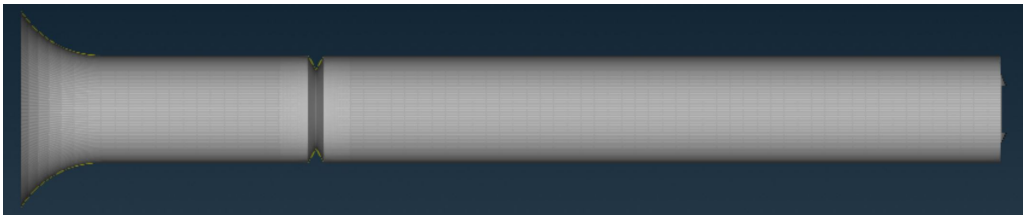

Figure 3.4: Shaft made out of AISI 316 steel with a v–notch of radius 0.03 mm subjected to cyclic rotating bending loading.

Model C

Figure 3.5: Tube made out of FeP04 drawing steel with a v–notch of radius 0.2 mm subjected cyclic axial loading.

Model D

Figure 3.6: Plate made out of 2024–T3 aluminium with a u–notch of radius 8.06 mm subjected cyclic axial loading.

3.2.2 Parameters and Test Data

The article by Yang et al. [34] did only provide the material parameters E, $H^{'}$ and n' for aluminium 7075–T6, which model A is made of. This data was therefore complemented with necessary material parameters, σ_{u}, $\sigma_{\mathrm{f}}^{'}$, b, $\epsilon_{\mathrm{f}}^{'}$ and c, from Boller & Seeger [25]. As for the AISI 316 steel used in model B, only the tensile strength, σ_{u}, was available in the article by Akita & Tokai [35]. The seven missing parameters were gathered from Boller & Seeger [24]. The parameters for the FeP04 drawing steel used in model C could all be gathered from the same article by Livieri et al. [36] that the geometry and test data was extracted from. As for the 2024–T3 aluminium used in model D, the parameters E, $\sigma_{\mathrm{f}}^{'}$, b, $\epsilon_{\mathrm{f}}^{'}$ and c were gathered from the original article by Moharram & Armin [37]. The three missing parameters were extracted from Boller & Seeger [25]. The resulting parameters from the process described above are all shown in table 3.1.
The test–data for, model A were extracted from the article by Yang et al. [34], model B from the article by Akita & Tokai [35], model C from the article by Livieri et al. [36] and model D from the article by Moharram & Armin [37]. In the latter article the test data were listed in tabular form which allowed for simple extraction. As for the other articles the test–data was only available in graphical form and the software WebPlotDigitizer [38] was used to extract the necessary data in numerical form. All articles contained data for reversed loading cycles but only the articles referencing model C and D contained test data for load cases with applied mean stress. The fatigue tests carried out with model C were carried out with a mean stress matching the amplitude to get a stress ration of $R = -1$. For model D however, the fatigue tests were instead carried out with constant mean stress for different amplitudes.

Table 3.1: Material and Fatigue Parameters.

Material	E	σ_{u}	$H^{'}$	$n^{'}$	$\sigma_{\mathrm{f}}^{'}$	b	$\epsilon_{\mathrm{f}}^{'}$	c
7075–T6	71420	572	1678	0.146	1048	-0.106	3.1357	-1.045
AISI 316	205000	576	691	0.154	660	-0.079	0.341	-0.453
FeP04	197000	552	502	0.0677	692	-0.078	33.7	-1.04
2024–T3	73100	490	557	0.039	927	-0.113	0.409	-0.713

3.2.3 Results, Linear–Elastic Material, Reversed Loading

The four different models presented in section 3.2 were evaluated with different loads applied corresponding to the test data available. The fatigue evaluation was done using the methodology laid out in section 3.1. The results for loading with reversed cycles, $R = -1$, are presented in figure 3.7, 3.8, 3.9 and 3.10. The modified approach by Morrow (MM) in equation 2.24, were compared with the approach suggested by SWT seen in equation 2.25 (see section 2.6.3). Red symbols represent the standard approach of evaluations based on stress and strain at the surface, green symbols represents using the point method (PM) with evaluation at a critical distance corresponding to the fatigue limit, and blue symbols represents using the PM with an iterated critical distance that matches the fatigue life.

The result for model A shows good correlation between experimental and analytical results. At higher nominal stress amplitudes, an improved accuracy was noted when applying the critical distance theory. This benefit was however not as prevalent at longer fatigue lives. Model B showed a massive improvement when applying the critical distance theory. This was expected since this model included the sharpest notch, 0.03 mm, in the case study. Since the test data is relatively close to the endurance limit the improvement by iteration is minor. Both model C and model D showed great correlation between experimental and analytical values while using the iterative solution of critical distance. Model D did not see much of an improvement when using the non–iterative approach which can be attributed to the blunt notch, 8.06 mm. However, the stresses applied to model D resulted in relatively low fatigue lives which means that the non–iterative approach of using k_{f} evaluated at the endurance limit is a majorly conservative assumption. This is further amplified by the fact that model D consists of aluminium with a presumed endurance limit of 5×10^8 cycles [1]. Therefore, the iterative approach improves the result significantly even though the notch is relatively blunt.

For all models, comparing the approach by Morrow and SWT does not yield any major differences. This is expected since no mean stresses have been applied. However the slight difference that is mainly observed in figures 3.7 and 3.10 is theorized by the authors to originate from the presence of plasticity at the evaluation point $L/2$. This is further discussed in chapter 4.

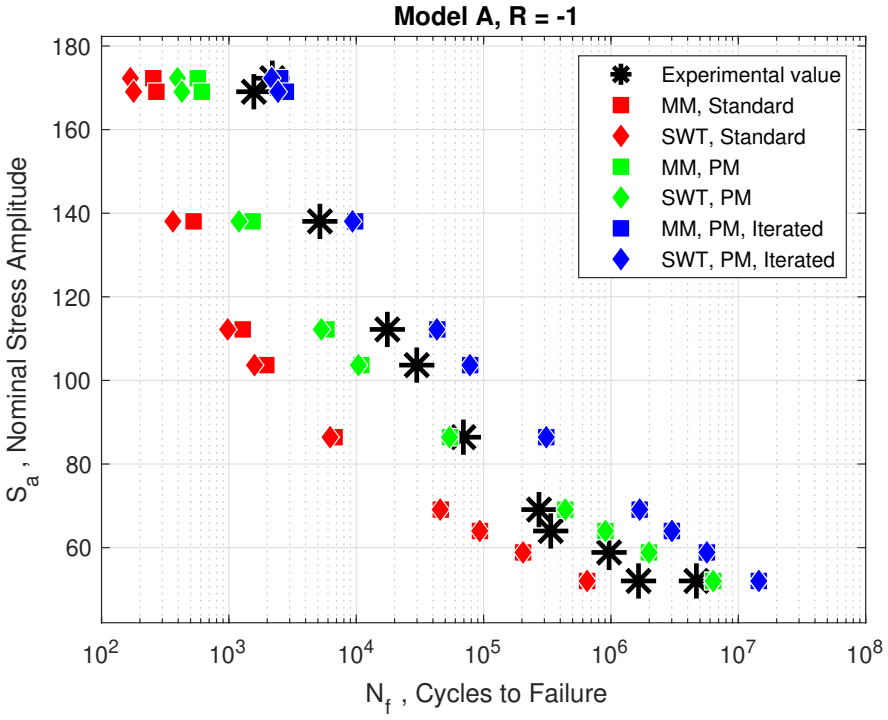

Figure 3.7: S–N comparison for Model A between experimental data and different approaches separated by different shape and colors of symbols. MM standing for Modified Morrow, SWT for Smith Watson & Topper, and PM for point method.

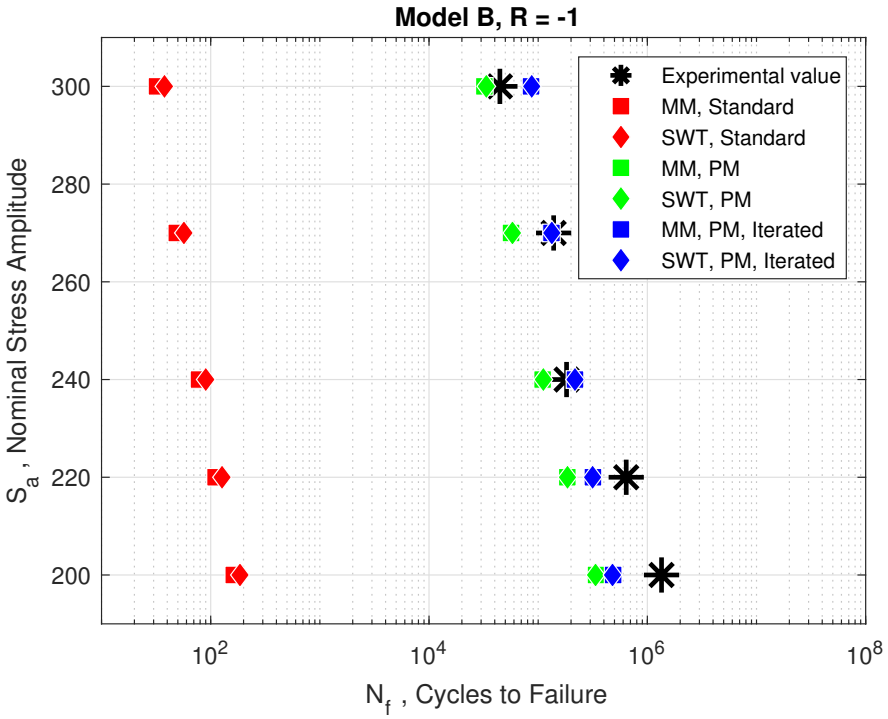

Figure 3.8: S–N comparison for Model B between experimental data and different approaches separated by different shape and colors of symbols.

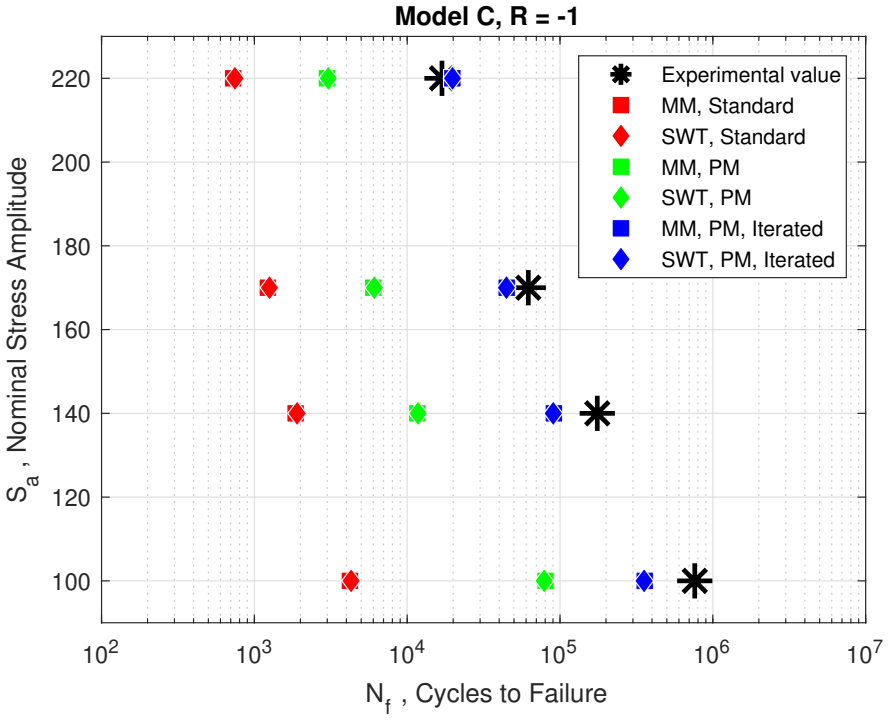

Figure 3.9: S–N comparison for Model C between experimental data and different approaches separated by different shape and colors of symbols.

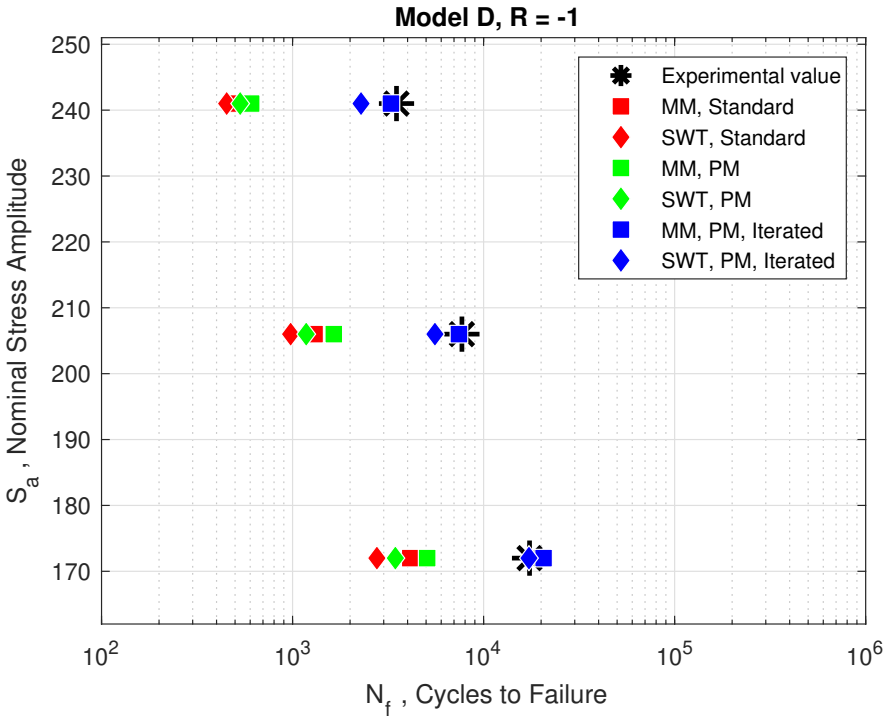

Figure 3.10: S–N comparison for Model D between experimental data and different approaches separated by different shape and colors of symbols.

3.2.4 Results, Linear–Elastic Material, Mean Stress Applied

The articles referencing model C and D contained test data for load cases with applied mean stress and were subsequently evaluated with the methodology laid out in section 3.1. These results are presented in fig 3.11 and 3.12. Model C showed good correlation between test data and analytical solution, especially at higher fatigue lives, and the benefit from iterating the critical distance is evident. The result for model D showed good correlation at lower mean stresses and acceptable results when increasing the mean stress. At increasing mean stresses the result has a conservative trend.

Comparing the approach by Morrow and SWT yields some differences, which might be attributed to the higher peak stresses associated with the addition of mean stress. This would make plasticity more probable. However, it is hard to draw conclusions from the limited data, especially since there is no clear trend throughout the results where one approach is more conservative than the other. For instance, comparing the approaches, the results show that SWT is more conservative at lower mean stresses while the trend shifts and Morrows approach is more conservative at larger mean stresses. This difference might be attributed to SWT compensating for mean stress in both terms, as stated in equation 2.23, while the modified approach by Morrow only compensates the 'first' term, as stated in equation 2.24.

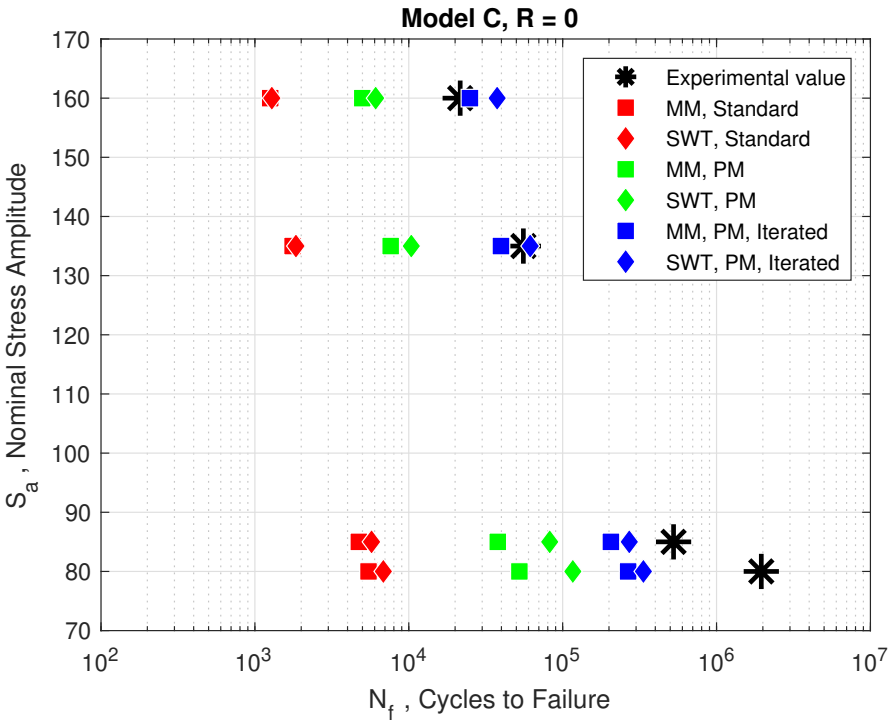

Figure 3.11: S–N comparison between different approaches and exp. data.

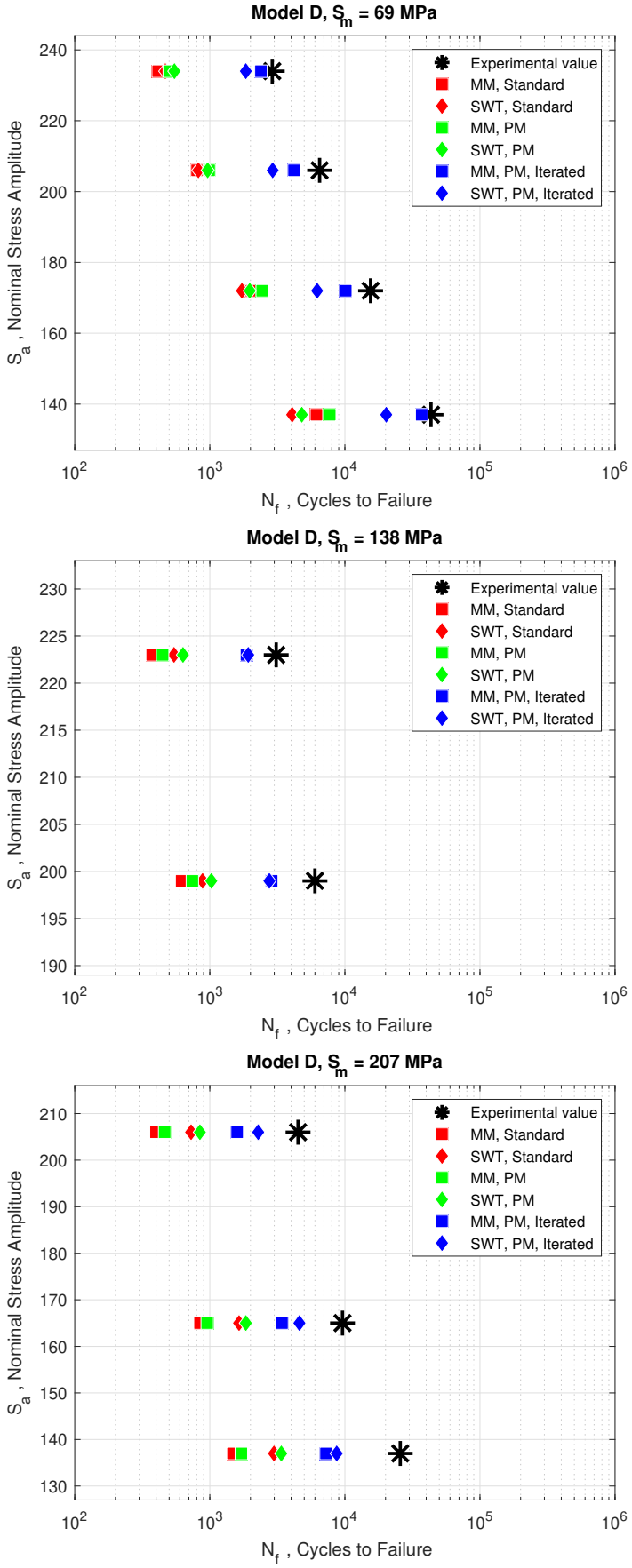

Figure 3.12: S–N comparison between different approaches and exp. data.

3.2.5 Results, Elasto–Plastic Material

Following the modifications to the linear-elastic procedure as presented in section 3.1.3, an elasto-plastic fatigue evaluation utilizing the TCD is possible. The plasticity model which is going to be used for this investigation is the multi–linear kinematic hardening model described in section 2.5.3. The input to the hardening model are found using equations 2.17 and 2.18 together with the material parameters H' and n' according to the procedure laid out at the end of section 2.5.3.

The results will be presented in plots comparing the experimental fatigue life, N_f with the predicted N_f. The plots will be divided both by stress ratio ($R = -1$ and $R \neq -1$) and mean stress correction (MM and SWT), meaning four plots will be shown. Figures 3.13 and 3.14 show results obtained using the Modified Morrow approach while the SWT approach is used in 3.15 and 3.16. The first figure of both approaches feature cases with a stress ratio of $R = -1$ while the second features results for tests and simulations with $R \neq -1$.

The fatigue predictions based on the fully reversed loading ($R = -1$) in figures 3.13 and 3.15 show no clear indication of any increased accuracy when using a plasticity model in the FEA. Instead, the linear–elastic FEA results clearly provided more accurate results compared to the plastic both when using the MM damage parameter (figure 3.13) and the SWT damage parameter (figure 3.15). The accuracy of the plastic results also seem to decrease at longer fatigue lives.

In figures 3.14 and 3.16 results from non–reversed loading ($R \neq -1$) are shown. Using the MM mean stress correction in conjunction with a plasticity model yielded excellent predictions at lower fatigue lives and acceptable predictions at larger N_f. Compared to the linear–elastic results there is a slight improvement in accuracy visible in figure 3.14. Using the SWT mean stress correction however yielded substantially less accurate results, with an increasing inaccuracy at longer lives. However, at shorter lives the predictions from both the linear–elastic and plastic FEA are acceptable. At longer lives, using a linear elastic material model seems to be more accurate here as well.

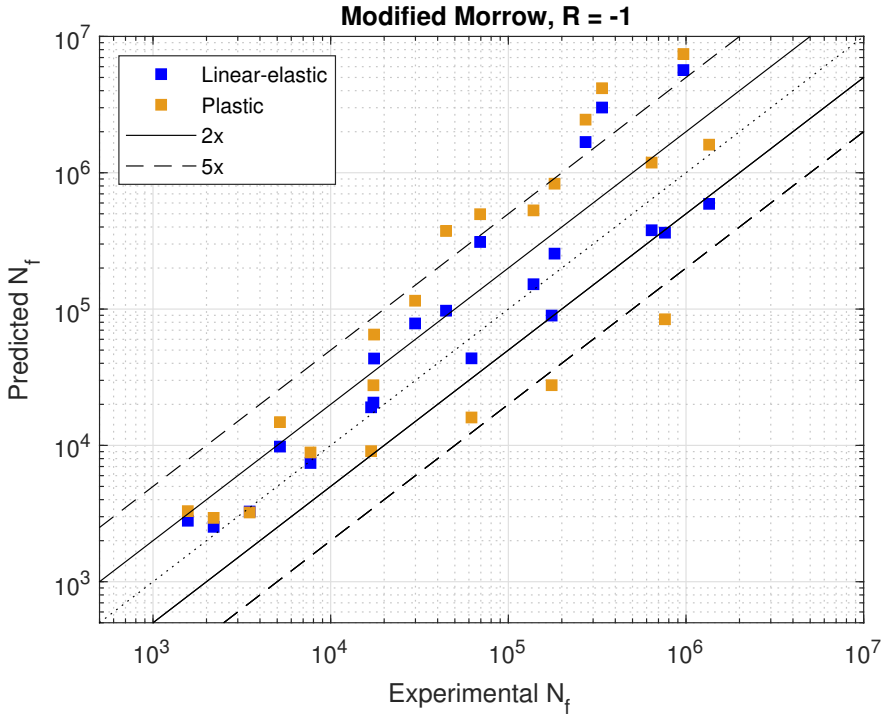

Figure 3.13: Comparison of fatigue predictions for tests with $R = -1$ using elastic and elasto–plastic material models and Modified Morrow mean stress correction

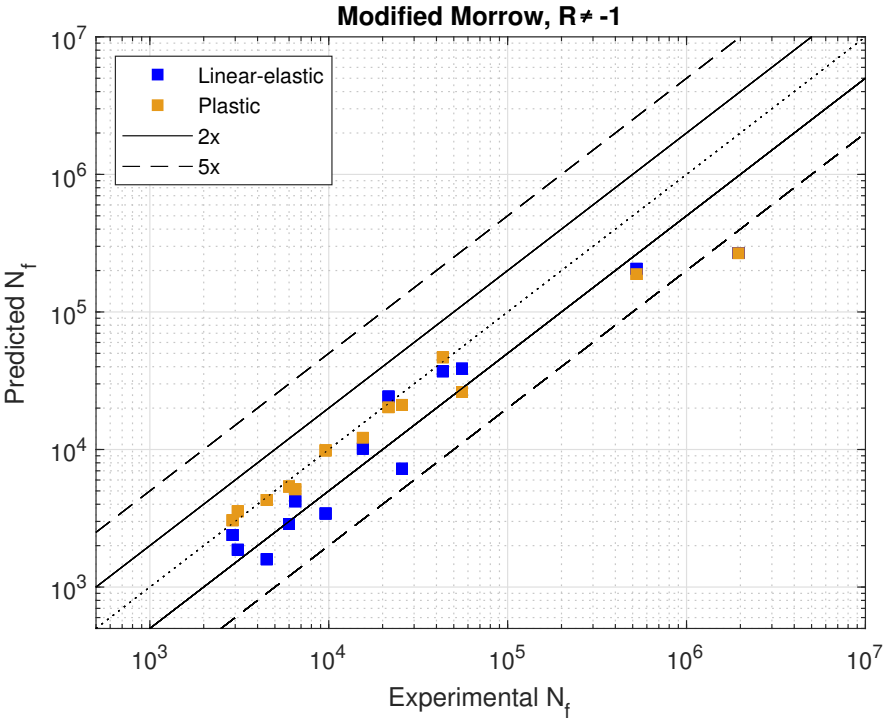

Figure 3.14: Comparison of fatigue predictions for tests with $R \neq -1$ using elastic and elasto–plastic material models and Modified Morrow mean stress correction.

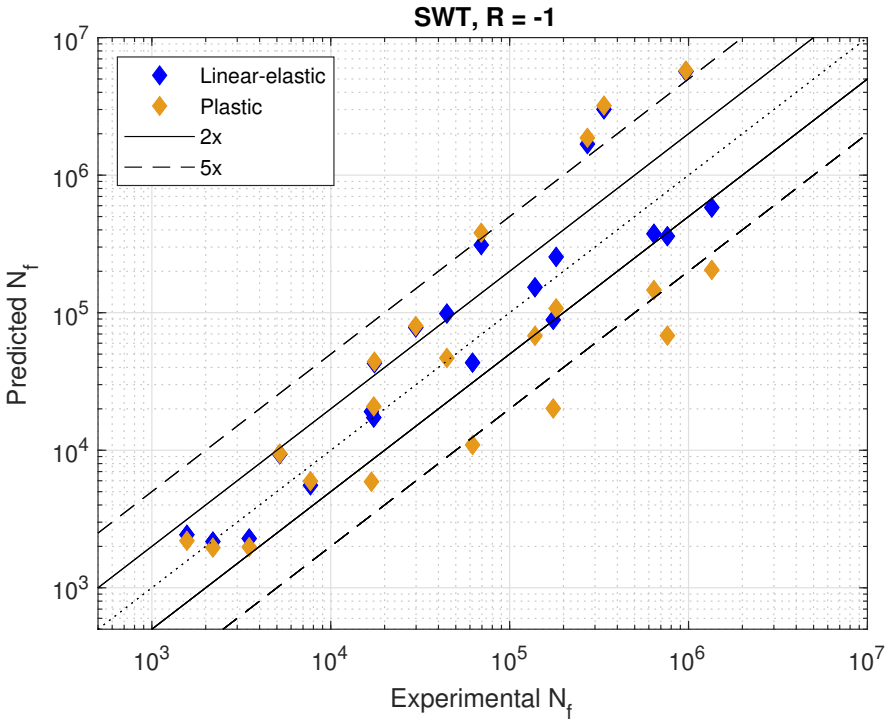

Figure 3.15: Comparison of fatigue predictions for tests with $R = -1$ using elastic and elasto–plastic material models and SWT mean stress correction

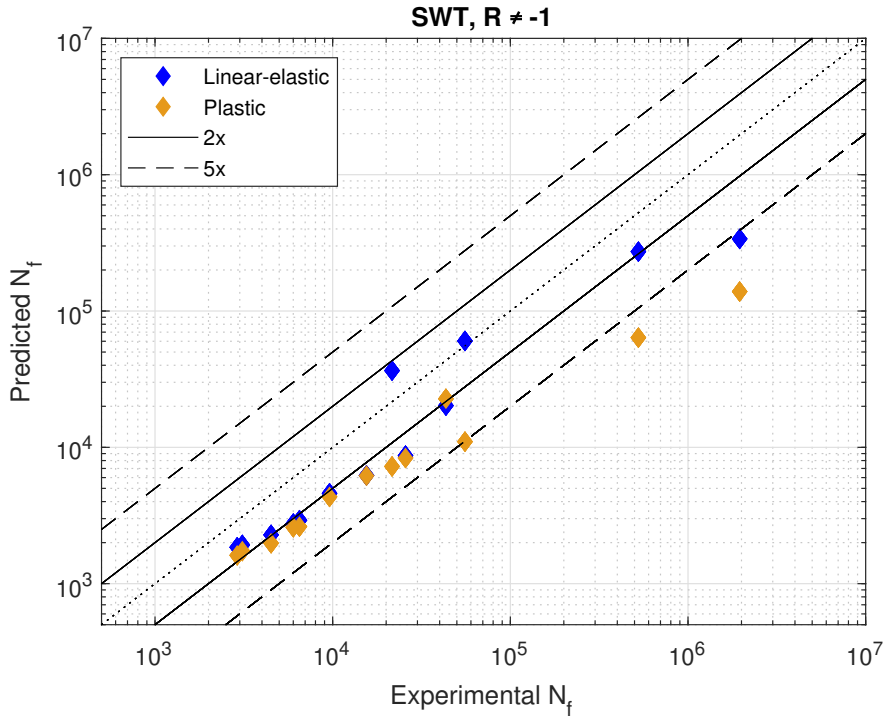

Figure 3.16: Comparison of fatigue predictions for tests with $R \neq -1$ using elastic and elasto-plastic material models and SWT mean stress correction.

3.3 Method Development – Complex Geometry

The methodology proposed in section 3.1 relies on the calculation of the fatigue notch factor, k_f, of the specific notch evaluated. Calculating k_f requires the theoretical stress concentration, k_t, to be known. It follows that in order to evaluate k_t a nominal stress has to be established, as per the definition in equation 2.1. However, components with more complex geometries might not have a defined nominal stress which would make the methodology proposed so far impossible to apply. Therefore, the authors developed another methodology, built on the same theory but without requiring the stress concentration factor.

3.3.1 The Application of Virtual Test Specimens

The methodology proposed sought inspiration from an article by David Taylor et al. [39] where a complex geometry had its critical distance evaluated by the employment of virtual test specimens. The virtual test specimens were of a defined material and simple geometry but with varied dimensions and notch geometry. A nominal stress was applied corresponding to the fatigue limit for each specimen and the stress distribution away from the notch was plotted. Figure 3.17 shows a demonstration of this with three virtual specimens made out of aluminium together with a horizontal line corresponding to the fatigue limit of a smooth specimen of the same material. The critical distance, $L/2$, for the virtual specimens can be observed to vary between 0.12 and 0.17 mm. A notch of similar geometry to the virtual specimens located in a complex geometry is assumed to have a similar critical distance. The authors therefore theorize that a good guess at the critical distance of the 'complex' notch would be the average of the critical distances of all virtual test specimens, with similar notches, employed. This calculation is presented in equation 3.1 where $L/2$ on the right represents the critical distance of the 'complex' notch.

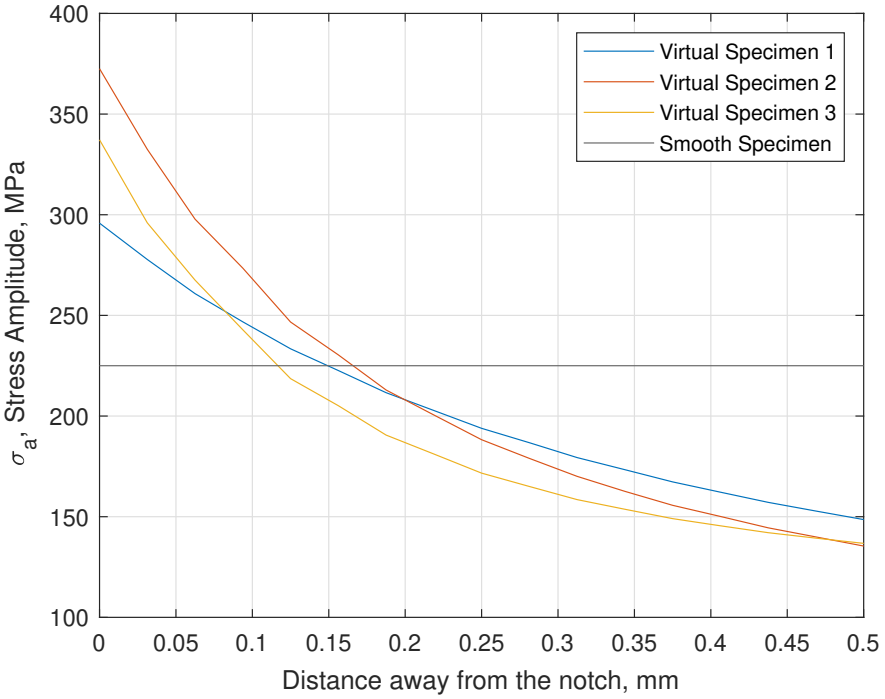

Figure 3.17: Graph showing the stress distribution away from the notch for different virtual specimens. The nominal stress has been scaled to correspond to the fatigue limit for each specimen.

$$\left(\sum_{i=1}^{n} \frac{L_i}{2}\right) \frac{1}{n} = \frac{L}{2} \tag{3.1}$$

3.3.2 Material Influence on Stress Distribution

This section will investigate to what extent the material parameters E and ν influence the shape and magnitude of the stress distribution ahead of the notch in a linear elastic analysis. If the influence is negligible it would mean that the stress data for the virtual test specimens would only have to be gathered once for an arbitrary material. This data could then be scaled accordingly to satisfy relations given by the notch fatigue factor for any given material. Since the scaling of stress distributions can be achieved without using FEA it would suggest that FEA would only be necessary for initial data gathering and not for future analysis using different materials. Testing was done by selecting a virtual test specimen and making linear elastic analysis of the stress distribution ahead of the notch while using different materials. The materials of choice were the materials used in the case studies and are shown in table 3.2 where the parameters of interest for the linear elastic analysis are listed as E and ν. The resulting stress distributions for the four different materials are shown in figure 3.18 and a magnification of the same figure is shown in figure 3.19. In the magnified figure it is clear that there is some difference between the stress distributions regarding different materials. The distance ahead of the notch that the same stress is achieved, represented by the intersections with the horizontal

line, differs for AISI 316 and any of the aluminiums by approximately 5 %. And this would result in a similar difference when calculating critical distance. However, the authors do not deem this a significant difference considering past experiences of working with the TCD aswell as the approximative and unreliable nature of fatigue predictions.

The material parameter with the largest influence on the stress distributions was identified as Poisson's ratio, ν. In figure 3.19 it can be observed how the metal with the intermediate value of ν, FeP04, is in the middle with the other metals offset by the approximately the same amount on each side which corresponds well to the difference in ν. The authors therefore conclude that when performing the linear elastic stress distribution analysis of the virtual test specimens a intermediate value of ν should be used. Reason being that the stress distribution should be as accurate as possible for the materials targeted. In this thesis the targeted materials were steels and aluminiums, similar to and including those in table 3.2, and ν were therefore given the intermediate value of 0.3.

Table 3.2: Mechanical and fatigue parameters.

Material	E [MPa]	ν
7075–T6	71420	0.33
AISI 316	205000	0.27
FeP04	197000	0.3
2024–T3	73100	0.33

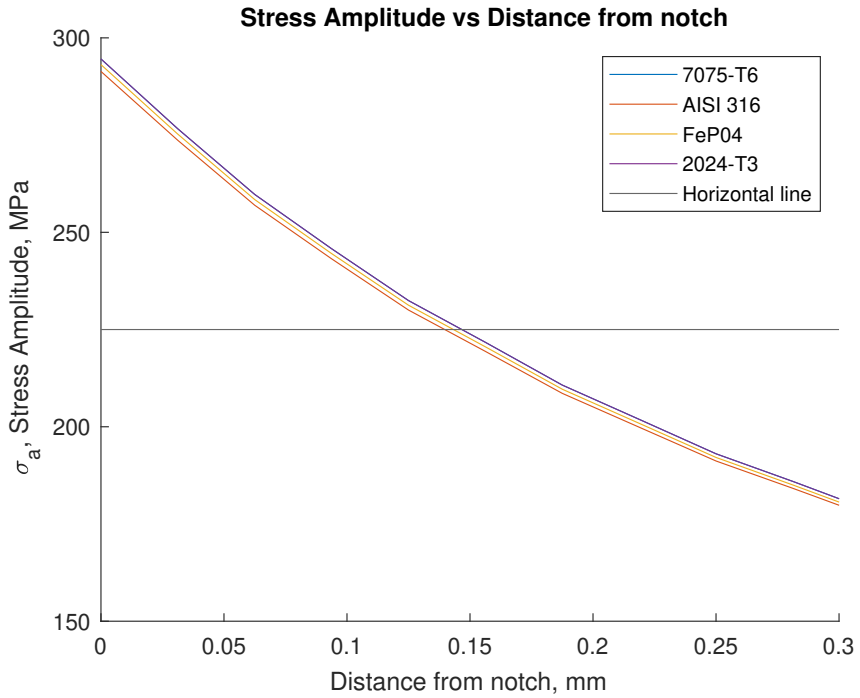

Figure 3.18: Graph showing the stress distribution away of the notch for different materials at identical loading.

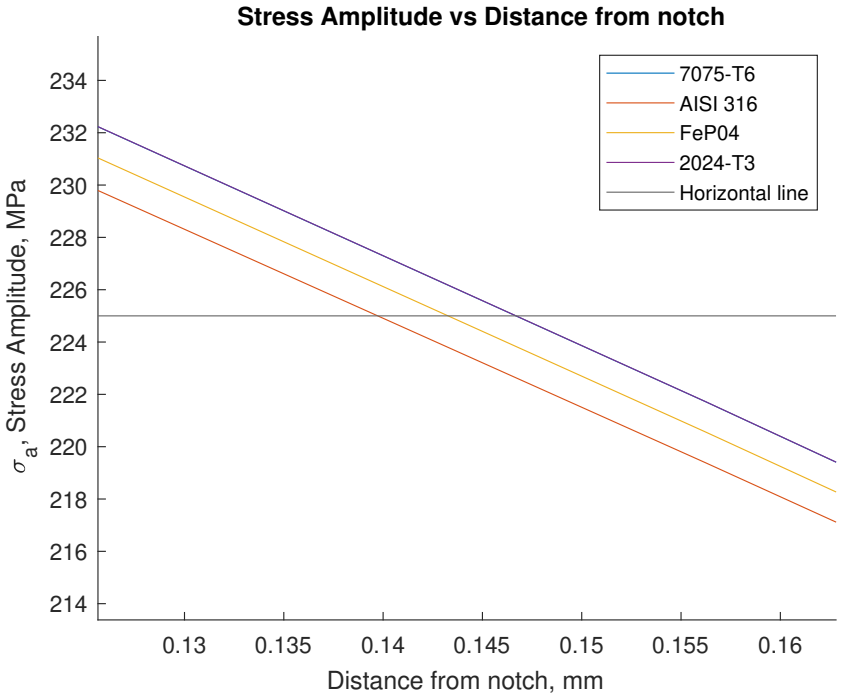

Figure 3.19: Magnified view over figure 3.18, the stress distribution of both aluminiums overlap.

3.3.3 The Construction of Virtual Test Specimens

A total of 16 different virtual test specimens were constructed, these are further described and presented in Appendix A. These include different u–notches, v–notches and holes where the notch radius was set to either 2 mm, 1 mm, 0.5 mm or 0.25 mm. Although the main purpose is laid out in section 3.3.4, another purpose of these specimens were to investigate the ranges that critical distance could vary within depending on geometry notch radius and material. The result can be viewed in figure 3.20 and 3.21 where the virtual specimens are applied nominal stresses corresponding to the fatigue limit for aluminium and steel, respectively. This was achieved by calculating k_f for each material and geometry which was then used to scale the stress distribution in MATLAB. It was not necessary to redo the FEA for each material for reasons laid out in section 3.3.2. The critical distances for aluminium shown in figure 3.20 can be observed to be generally larger than those corresponding to steel in figure 3.21. This correlates well with the higher notch sensitivity associated with ductile materials visible in figure 2.5. The critical distance for virtual specimens made out of aluminium varies between approximately 0.075 and 0.18 which can be considered a significant spread. However, the authors suggests a selective approach to narrow the spread which is laid out in section 3.3.4.

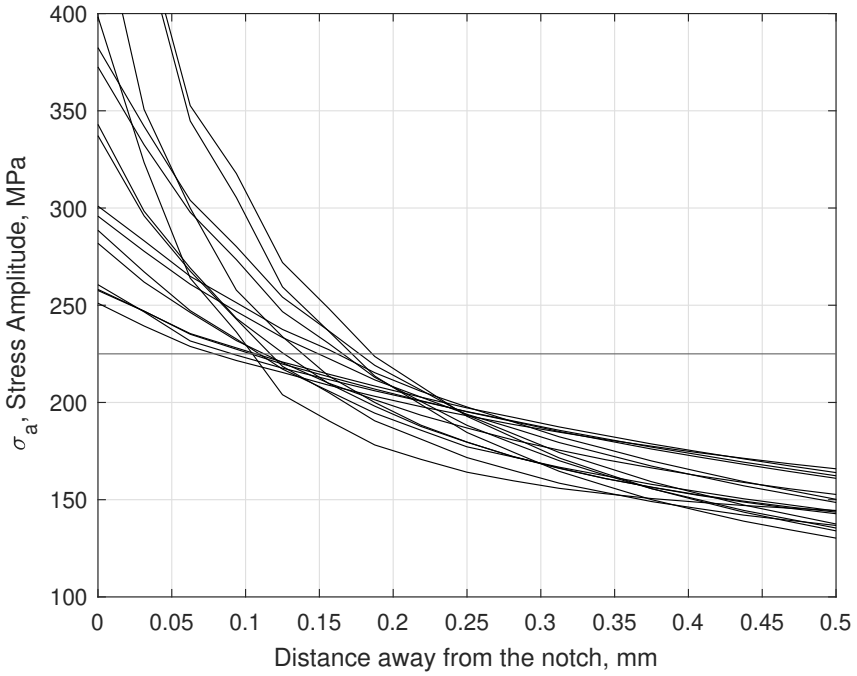

Figure 3.20: Graph showing the stress distribution away from the notch for different virtual specimens made out of 2024–T3 aluminium. The nominal stress is scaled to correspond to the fatigue limit for each specimen.

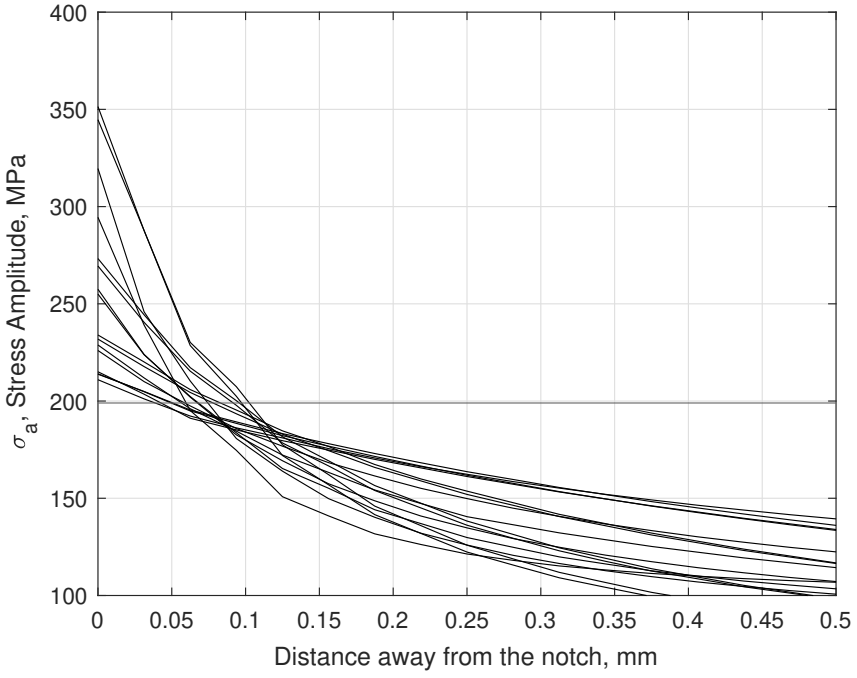

Figure 3.21: Graph showing the stress distribution away from the notch for different virtual specimens made out of AISI 316 steel. The nominal stress is scaled to correspond to the fatigue limit for each specimen.

3.3.4 Selective Approach to Virtual Test Specimens

The different stress distributions in figure 3.20 and 3.21 produce a significant spread in critical distance which can be attributed to the different geometries and notch radii. Since the radius of a 'complex' notch and the general geometry involved usually is known, a selection for virtual test specimens of similar features should be made. This will allow for a more accurate and narrow spread of the 'virtual' critical distances employed for calculating the 'complex' critical distance through equation 3.1.

In the first example, a complex geometry made out of 2024–T3 aluminium featuring a tight hole is to be evaluated. Deactivating all specimens that do not resemble a hole results in the graph presented in figure 3.22. The deactivated specimen have their stress distributions greyed out while the still active specimens remain black. The graph shows that the critical distance is now narrowed down to between 0.103 and 0.117 mm. Equation 3.1 evaluates the average final value;

$$\left(\sum_{i=1}^{n} \frac{L_i}{2}\right) \frac{1}{n} = (0.103 + 0.104 + 0.109 + 0.117)\frac{1}{4} = 0.108\,\text{mm}$$

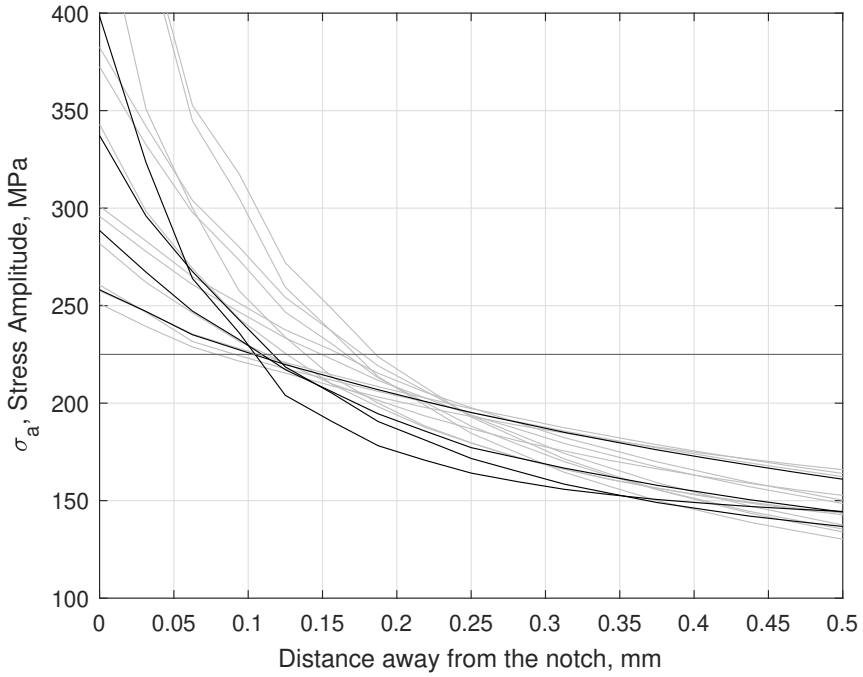

Figure 3.22: Stress distributions away from the notch for different virtual specimens made out of 2024–T3 aluminium. The nominal stress is scaled to correspond to the fatigue limit for each specimen. Deactivated specimens are greyed out.

Another conclusion from figure 3.22 is that the critical distance is relatively small for all 'hole' specimens regardless of notch radius. However, the 'notch' specimens

do not follow the same trend and the authors therefore conclude there are significant differences between the stress distributions of holes and notches. It follows that these should not be mixed when using the selective approach to virtual test specimens.

Example 2: A complex geometry made out of 2024–T3 aluminium includes a notch with a radius between 0.25 and 0.5 mm. All 'hole' specimens and specimens with a notch radius of 1 and 2 mm are deactivated. The resulting graph is shown in figure 3.23. The critical distance is narrowed down to between 0.127 and 0.186 mm with some weight towards the larger value. The average distance is evaluated as;

$$\left(\sum_{i=1}^{n} \frac{L_i}{2}\right) \frac{1}{n} = (0.127 + 0.138 + 0.166 + 0.172 + 0.177 + 0.186)\frac{1}{6} = 0.161 \text{ mm}$$

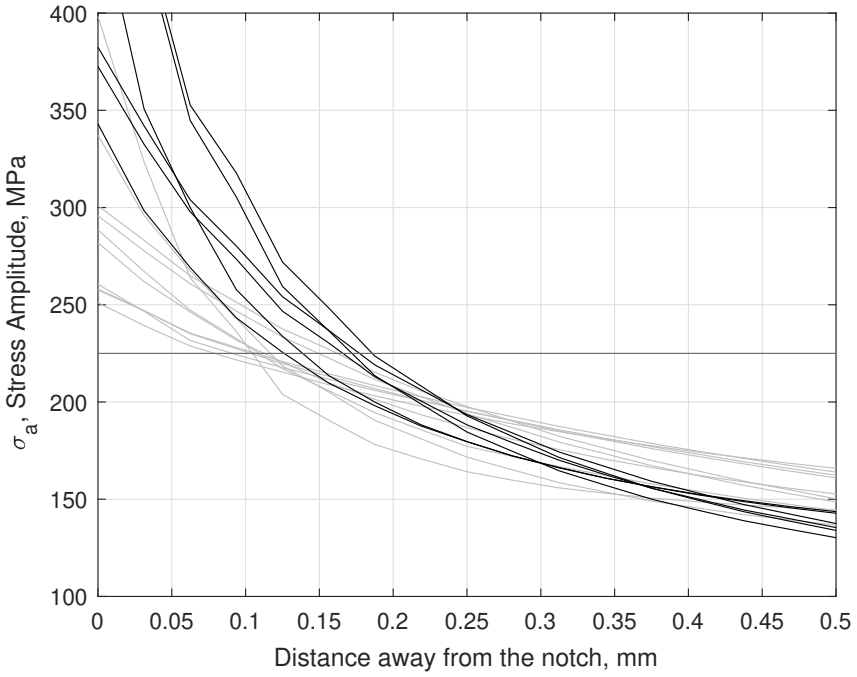

Figure 3.23: Stress distributions away from the notch for different virtual specimens made out of 2024–T3 aluminium. The nominal stress is scaled to correspond to the fatigue limit for each specimen. Deactivated specimens are greyed out.

3.3.5 Proposed Methodology

In this section the whole procedure for evaluating the fatigue life of a notch in a complex geometry is laid out. This process is shown as a flowchart in figure 3.24. The first step is to study the geometry around the notch and the notch itself in order get an understanding of what virtual test specimens that are suitable to employ in the next step. Once the irrelevant virtual specimens have been deactivated the goal is to scale the stress distributions so that all virtual specimens have a fatigue

life of $N_{f,ref}$. This is done by calculating $k_{f,ref}$ for each specimen using the material parameters, q and σ_u, of the original component of complex geometry. Similarly to the proposed methodology for simple geometry described in section 3.1.2, the initial value of $N_{f,ref}$ is not that significant since it is just a starting point for the iteration process. However, if no iteration is to be employed, using the endurance limit will ensure a conservative assumption of $k_{f,ref}$. Once $k_{f,ref}$ is determined it is possible to scale the nominal stresses, and therefore the stress distributions, of the virtual specimens so that they all have the identical fatigue life of $N_{f,ref}$. The next step is plotting the stress distributions of all activated virtual specimens, as shown in figure 3.23, and determining the critical distance for each specimen. The critical distances are then employed in equation 3.1 where an average value is calculated and will serve as an estimation of what the critical distance should be at the notch of the complex geometry. Using this averaged critical distance, the point of evaluation is determined for the complex component. The following process of calculating the fatigue life of the complex component is then identical to the process described in section 3.1.2. Due to difficulties in obtaining fatigue test data for complex geometries there were no case studies done utilizing this process.

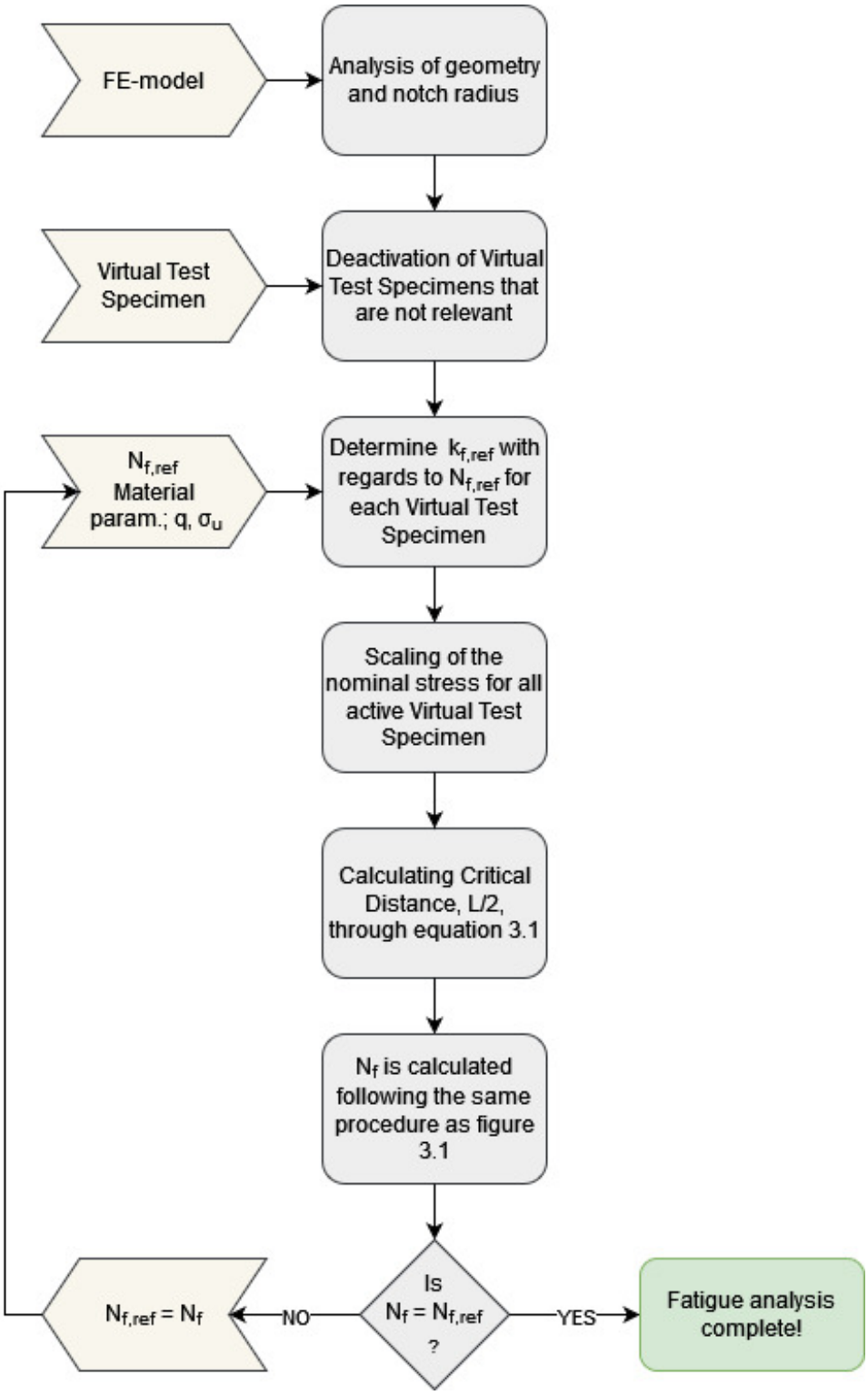

Figure 3.24: Flowchart

4

Discussion

As explained, calculation of $k_{\mathrm{f,ref}}$ is done through interpolation between $k_{\mathrm{f}}^{'}$ at 1000 cycles and k_{f} at the endurance limit. The problem is that while most steels have a distinct endurance limit, non–ferrous materials such as aluminium do not. However, when designing using aluminium it is common to assume that there in fact is an endurance limit [1]. Two of the models, A and D, in the case studies were made of aluminium and thus an assumption of an endurance limit had to be done. Dowling [1] recommends an endurance limit of 5×10^8 which was used throughout the work. This assumed endurance limit might be too large and other sources assumes a lower number of cycles at 5×10^7 [40]. The impact of the assumed endurance limit for the aluminium will be most notable at longer fatigue lives, which model A has the most of. Assuming figure 3.7 were to be reconstructed, using the assumption of 5×10^7 cycles, the blue symbols notating the results obtained using iteration would more quickly with an increasing fatigue life approach the results obtained using the critical distance at the endurance limit, i.e. the green symbols. This not only means that the fatigue predictions could have been more accurate for model A, but also serves as a reminder for how some of the inevitable assumptions that have to be made in fatigue evaluations could have a large impact on the results.

The result for the non–reversed load case ($R \neq -1$) of model D in figure 3.12 shows a conservative trend with increasing mean stress. This divergence from the more accurate result for the simple load case in figure 3.10 might be attributed to a shortcoming in the plasticity correction employed in the linear elastic approach. This is because of higher peak stresses associated with increasing mean stress which would induce more plasticity. And it follows that if more plasticity is present the correction for it has a larger influence on the result. The correction is executed using the Neuber rule as laid out by Dowling [1]. The simplicity of this approach or less than ideal values of $K^{'}$ and $n^{'}$ could help explain the conservative trend observed in figure 3.12. The Neuber Rule seem to operate optimally under plane stress conditions which the stress state at the surface of the component bears a strong resemblance to. However, since the Theory of Critical Distances moves the location of evaluation slightly into the component it is possible that this condition is to some degree altered. This might also influence the accuracy of the plasticity correction employed. But in the case of model D the test specimen can be considered a thin flat plate which is usually associated with a global plane stress condition. The authors therefore think that in the case of model D, the plane stress condition still applies.

In this report, the authors also set out to investigate the usage of a plasticity model in

the FEA in conjunction with the proposed methodology. A simpler multi–linear plasticity model was chosen which was calibrated using the plastic part of the Ramberg–Osgood form shown in equation 2.17. This decision was motivated due to the more complex plasticity models requiring an increased number of material parameters which were difficult to acquire. This means that finding the necessary parameters for each material would simply not be feasible without performing material tests. Because the approach to plastic FEA taken in this report is simple, mostly due to the fact that the only required material parameters are $K^{'}$ and $n^{'}$ which are very common, it might not be complex enough to draw any conclusions about the applicability of plasticity models together with the TCD. It did however increase the computational times from a few minutes in the linear–elastic analyses to over an hour in most cases for the elasto–plastic. This means that the computational times essentially was increased by a factor of 10–30 with no benefit in terms of accuracy.

While validating the method for simple geometry in section 3.1 two different mid stress corrections were utilized. The approach by Modified Morrow, equation 2.24, were compared with the approach by SWT presented in equation 2.23. For some case study results there were little to no difference between the both of them as shown in figure 3.8 and 3.9. The authors speculate that this is because of the similarity of both damage functions and lack of plasticity at the location of evaluation. The modified Morrow mid stress correction model uses strain while SWT utilizes both the stress and strain. While there is a linear relationship between the stress and strain as well as no mid stresses present it should have no effect if the damage is calculated using either one or both of them. However, when plasticity is introduced the stress and strain instead follows the Ramberg–Osgood relation where strain becomes more 'dominant'. It follows that the evolution regarding the value of the damage parameters will differ as more plasticity is introduced. The authors, on the basis of the result from the case studies, do however not give a conclusive judgement on whether the approach by Modified Morrow or SWT is preferred.

Material parameters, and certain modelling assumptions, have a great impact on the resulting fatigue predictions. In section 3.2, the authors of this report explains the reasoning behind the evaluation reliability of the parameters. Ideally the employed literature would contain all the necessary material and fatigue parameters (listed in table 3.1). While not all articles contained a complete set of the required parameters, all of them provided at least some common parameters for describing the material behaviour. A strong match of the processing and heat treatment between the research paper containing the parameters and the research paper containing the fatigue test data would be the second best alternative in cases where none of the required parameters are provided. This way one could expect the material used in both research papers to be similar in their behaviour. Unfortunately, such information have been scarce in the investigated articles and thus other factors had to be prioritized. A good correlation between the earlier mentioned common parameters such as Young's modulus E, the ultimate tensile strength σ_{u}, and the yield strength σ_{y}, were sought after. During the process of searching for sources with good correlation, the different sets of parameters were tested. The predicted fatigue life could

vary with several orders of magnitude, which clearly showcases the importance of reliable parameters and the uncertainties involved with fatigue evaluations as a whole.

It is also important to keep in mind the uncertainties involved with cyclic fatigue tests. Figure features a very clear example where the fatigue life of the specimen subjected to a nominal stress amplitude of 172 MPa was 2194 cycles while the specimen subjected to a nominal stress amplitude of 169 MPa had a fatigue life of 1570 cycles. There are many different reasons to such irregular behaviour such as manufacturing defects and attachment of the specimen in the test machine. Due to uncertainties like these, results indicating incredible accuracy such as the ones shown in figure 3.10 must be taken with caution.

As mentioned in section 3.3, the developed methodology had to be expanded to allow for fatigue predictions of complex geometries. This methodology has thus far not been validated against any test data, due to time limitations and a lack of fatigue test data for complex geometries. Therefore no conclusions could be drawn about the applicability of the method. The authors also believe that the collection of virtual test specimens would have to be expanded. One reason for this could be explained using figure 2.1, where k_t clearly depends on the notch radius, but also on other geometrical factors. Simply put, the stress concentration is dependant on the size and geometry of the whole component. The 16 different modelled virtual test specimens include different notch types and radii. However, the overall size and other geometrical relations as well as an axial loading case have been kept similar due the sharp increase in number of test specimens necessary to include these factors.

The authors also theorize that one possible solution would be to construct a few virtual specimen on demand which would represent the notch or sharp corner in the component investigated. This way, there would be no need for a large database of virtual test specimen which would be very time consuming to create. The methodology would then be very similar to the one laid out in section 3.3.5 which also is visualised with the flowchart in figure 3.24. What would differ the two variants of the methodology is that instead of deactivating virtual test specimen that are deemed irrelevant, new test specimens would be created to resemble the notch and stress–strain state around it.

The mesh density is a factor which could have a large influence on the resulting stress–strain state. It would have been interesting to also consider which influence the mesh density has on the accuracy of the proposed methodology. However, the meshes were constructed to be very fine close to the notch to allow for a higher resolution of the stress distributions. The authors therefore deem the mesh and its optimization a question better brought up in the future, when design guidelines including mesh parameters are to be established.

The environmental and economical potential of utilizing the proposed methodology was touched upon in the introduction. When the fatigue evaluations are conservative the severity of the notch is overestimated which means that the geometry might

have to be reinforced to lower the nominal stresses acting on the notch. Another impact of overestimating the severity of notches reveals itself when entire solutions or designs would be scrapped due to not fulfilling fatigue requirements. It follows that if more accurate evaluations were employed, whole structures or components could be dimensioned using less material, and opportunities for more attributes to be optimized would be discovered.

This thesis was conducted with the cooperation of VCC with an aim of equipping the organisation with a better tool for fatigue evaluation of notches. Since VCC is making a transition towards 100 % electric vehicles by 2030 [41], the methodology proposed by the authors could influence the success of this transition with the environment reaping the benefits of putting electric cars on the market.

5
Conclusion

This report sought to investigate and develop a methodology for predicting fatigue in sharp corners and notches in a less conservative manner. The authors deemed the Theory of Critical Distances to be a promising concept which was further investigated. A methodology, based on the TCD was developed capable of predicting fatigue in notches with good accuracy for simple geometries. Not surprisingly, considering the concept of notch sensitivity introduced in section 2.3.2, the proposed methodology and its supporting theory becomes increasingly important to consider when the material is more ductile and the notch radius is small.

The authors found no conclusive evidence as to whether elasto–plastic FEA or linear–elastic FEA is more accurate to use in the proposed methodology. This could be seen as an indication that the increased computational power and complexity associated with plasticity models might not be necessary. With this in mind, the authors recommend not using plasticity models in FEA, at least in conjunction with the proposed methodology.

To take the first steps for implementation into the CAE toolbox at Volvo Cars, the authors extended the methodology to also include possibilities for predictions in more complex geometries. This was done through the utilization of so called virtual test specimens. The concept behind this is presented in the report but the accuracy could not be validated, both due to time limitations and difficulties in finding fatigue test data with relevant geometries. However, some conclusions could be made, the estimated critical distance of a virtual test specimen was shown to vary significantly depending on notch geometry and this effect was more prevalent in ductile materials. This emphasizes the importance of utilizing relevant notch geometries when employing virtual test specimen. The authors therefore deem the alternative approach discussed under chapter 4 to be particularly interesting, where virtual test specimen would be created on demand. This would allow for creating exclusively relevant virtual test specimens, tailored to represent the notch which is to be evaluated. But further research and validation of the employment of virtual test specimen is necessary for a more accurate assessment of its viability.

Bibliography

[1] Norman E Dowling, Stephen L Kampe, and Milo V Kral. *Mechanical behavior of materials*. Pearson Education Ltd, 5 edition, 2020.

[2] NE Frost. A relation between the critical alternating propagation stress and crack length for mild steel. *Proceedings of the Institution of Mechanical Engineers*, 173(1):811–836, 1959.

[3] *ABAQUS Materials User's Guide, Version 2021*. Dassault Systemes Simulia Corp, United States, 2020.

[4] Ayhan Ince and G. Glinka. A numerical method for elasto-plastic notch-root stress–strain analysis. *The Journal of Strain Analysis for Engineering Design*, 48:229–244, 04 2013.

[5] Ayhan Ince and Grzegorz Glinka. A generalized fatigue damage parameter for multiaxial fatigue life prediction under proportional and non-proportional loadings. *International Journal of Fatigue*, 62:34–41, 2014. 9th Fatigue Damage of Structural Materials Conference.

[6] David Taylor. Analysis of fatigue failures in components using the theory of critical distances. *Engineering Failure Analysis*, 12(6):906–914, 2005. Papers presented at the First International Conference on Engineering Failure Analysis (Lisbon, Portugal, 12–14 July 2004). Part II.

[7] Heinz Neuber. Theory of notch stresses : principles for exact calculation of strength with reference to structural form and material. 1958.

[8] Rudolph Eearl Peterson. Notch sensitivity. *Metal fatigue*, pages 293–306, 1959.

[9] Luca Susmel and Daisey Taylor. A novel formulation of the theory of critical distances to estimate lifetime of notched components in the medium-cycle fatigue regime. *Fatigue & Fracture of Engineering Materials & Structures*, 30:567 – 581, 06 2007.

[10] Shun-Peng Zhu, Jin-Chao He, Ding Liao, Qingyuan Wang, and Yongjie Liu. The effect of notch size on critical distance and fatigue life predictions. *Materials & Design*, 196:109095, 2020.

[11] Nicholas R. Gates and Ali Fatemi. Multiaxial variable amplitude fatigue life analysis using the critical plane approach, part ii: Notched specimen experiments and life estimations. *International Journal of Fatigue*, 106:56–69, 2018.

[12] T. H. Topper, R. M. Wetzel, and J. Morrow. Neuber's rule applied to fatigue of notched specimens. 1967.

[13] David Taylor. *The theory of critical distances: A new perspective in fracture mechanics*. Elsevier, 2007.

[14] Ding et al. Liao. Recent advances on notch effects in metal fatigue: A review. *Fatigue & Fracture of Engineering Materials & Structures*, 43(4):637–659, 2020.

[15] David Taylor. Geometrical effects in fatigue: a unifying theoretical model. *International Journal of Fatigue*, 21(5):413–420, 1999.

[16] Daniel Bellett, David Taylor, Stefano Marco, Ezio Mazzeo, Jerome Guillois, and Thomas Pircher. The fatigue behaviour of three-dimensional stress concentrations. *International Journal of Fatigue*, 27(3):207–221, 2005.

[17] P. Lukás, L. Kunz, B. Weiss, and R. Stickler. Notch size effect in fatigue. *Fatigue & Fracture of Engineering Materials & Structures*, 12(3):175–186, 1989.

[18] ANDREA CARPINTERI, A. SPAGNOLI, and S. VANTADORI. An approach to size effect in fatigue of metals using fractal theories. *Fatigue & Fracture of Engineering Materials & Structures*, 25(7):619–627, 2002.

[19] M. Shirani and G. Härkegård. Fatigue life distribution and size effect in ductile cast iron for wind turbine components. *Engineering Failure Analysis*, 18(1):12–24, 2011.

[20] H. Neuber. Theory of Stress Concentration for Shear-Strained Prismatical Bodies With Arbitrary Nonlinear Stress-Strain Law. *Journal of Applied Mechanics*, 28(4):544–550, 12 1961.

[21] W. N. Sharpe, C. H. Yang, and R. L. Tregoning. An evaluation of the Neuber and Glinka relations for monotonic loading. *Journal of Applied Mechanics*, 59(2S), 1992.

[22] M Knop and et al. On the Glinka and Neuber methods for calculating notch tip strains under cyclic load spectra. *International Journal of Fatigue*, 22(9):743–755, 2000.

[23] G. Glinka. Energy density approach to calculation of inelastic strain-stress near notches and cracks. *Engineering Fracture Mechanics*, 22(3):485–508, 1985.

[24] Chr Boller and T Seeger. *Materials data for cyclic loading - Part C: High-alloy Steels*. Elsevier, 1 edition, 1987.

[25] Chr Boller and T Seeger. *Materials data for cyclic loading - Part D: Aluminium and Titanium alloys*. Elsevier, 1 edition, 1987.

[26] Ayhan Ince. *Development of Computational Multiaxial Fatigue Modelling For Notched Components*. PhD thesis, University of Waterloo, Waterloo, Ontario, Canada, 2012.

[27] A Fatemi and RI Stephens. Tensile mean stress effects on uniaxial fatigue behavior of 1045 hr steel. *Fatigue'87.*, 1:537–546, 1987.

[28] Hitoshi Soyama, Christopher R. Chighizola, and Michael R. Hill. Effect of compressive residual stress introduced by cavitation peening and shot peening on the improvement of fatigue strength of stainless steel. *Journal of Materials Processing Technology*, 288:116877, 2021.

[29] Tianwen Zhao, Jixi Zhang, and Yanyao Jiang. A study of fatigue crack growth of 7075-t651 aluminum alloy. *International Journal of Fatigue*, 30(7):1169–1180, 2008.

[30] D. F. Socie and JoDean Morrow. *Review of Contemporary Approaches to Fatigue Damage Analysis*, pages 141–194. Springer US, Boston, MA, 1980.

[31] K.N. Smith et.al. A stress–strain function for the fatigue of metals (stress-strain function for metal fatigue including mean stress effect). *J Materials*, 5:767–778, 1970.

[32] Masayuki Kamaya and Masahiro Kawakubo. Loading sequence effect on fatigue life of type 316 stainless steel. *International Journal of Fatigue*, 81:10–20, 2015.

[33] C. Amzallag, J.P. Gerey, J.L. Robert, and J. Bahuaud. Standardization of the rainflow counting method for fatigue analysis. *International Journal of Fatigue*, 16(4):287–293, 1994.

[34] Yang Ai, Shun-Peng Zhu, Ding Liao, José A.F.O. Correia, Abílio M.P. De Jesus, and Behrooz Keshtegar. Probabilistic modelling of notch fatigue and size effect of components using highly stressed volume approach. *International Journal of Fatigue*, 127:110–119, 2019.

[35] Masayuki Akita and Keiro Tokaji. Effect of carburizing on notch fatigue behaviour in aisi 316 austenitic stainless steel. *Surface and Coatings Technology*, 200(20):6073–6078, 2006.

[36] P. Livieri, E. Salvati, and R. Tovo. A non-linear model for the fatigue assessment of notched components under fatigue loadings. *International Journal of Fatigue*, 82:624–633, 2016.

[37] Moharram Mohammadi and Armin Rahmatfam. Low-cycle fatigue life prediction assessment of notched aluminum 2024-t3 under cyclic axial loading. *Ships and Offshore Structures*, 0(0):1–11, 2021.

[38] Ankit Rohatgi. Webplotdigitizer: Version 4.5, 2021.

[39] D. Taylor, P. Bologna, and K. Bel Knani. Prediction of fatigue failure location on a component using a critical distance method. *International Journal of Fatigue*, 22(9):735–742, 2000.

[40] J. Carvill. 1 - strengths of materials. In J. Carvill, editor, *Mechanical Engineer's Data Handbook*, pages 1–55. Butterworth-Heinemann, Oxford, 1993.

[41] Volvo cars to be fully electric by 2030. *Volvo Cars Global Newsroom*, Mar 2021.

A

Appendix 1

The 16 Virtual Test Specimen were constructed using the four different geometries presented below where for each geometry the notch radius was varied between 0.25, 0.5, 1 and 2 mm. In the figures below the notch radius are 2 mm for all specimen. The specimen have the characteristics of a plate with thickness 2 mm and a length of 160 mm. The specimen were constructed with a symmetry plane along the bottom side if viewed from the orientation presented below. This allows for a symmetric specimen that is not bent during the applied horizontal axial force.

U-Notch (180 °) Virtual Test Specimen

V-Notch Virtual Test Specimen

U-Notch (90 °) Virtual Test Specimen

Hole Virtual Test Specimen

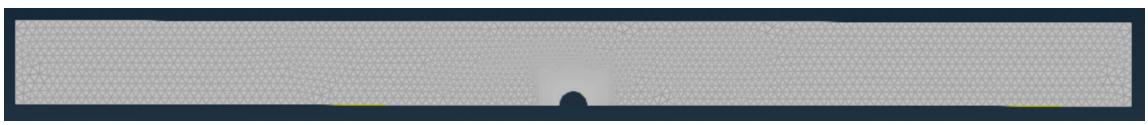

DEPARTMENT OF SOME SUBJECT OR TECHNOLOGY
CHALMERS UNIVERSITY OF TECHNOLOGY
Gothenburg, Sweden
www.chalmers.se

CHALMERS
UNIVERSITY OF TECHNOLOGY